PHYSICAL REVIEW B **87**, 075145 (2013)

Quantum phase transitions in a pseudogap Anderson-Holstein model

Mengxing Cheng* and Kevin Ingersent
Department of Physics, University of Florida, Gainesville, Florida 32611-8440, USA
(Received 12 January 2013; published 26 February 2013)

We study a pseudogap Anderson-Holstein model of a magnetic impurity level that hybridizes with a conduction band whose density of states vanishes in power-law fashion at the Fermi energy, and couples, via its charge, to a nondispersive bosonic mode (e.g., an optical phonon). The model, which we treat using poor-man's scaling and the numerical renormalization group, exhibits quantum phase transitions of different types depending on the strength of the impurity-boson coupling. For weak impurity-boson coupling, the suppression of the density of states near the Fermi energy leads to quantum phase transitions between strong-coupling (Kondo) and local-moment phases. For sufficiently strong impurity-boson coupling, however, the bare repulsion between a pair of electrons in the impurity level becomes an effective attraction, leading to quantum phase transitions between strong-coupling (charge Kondo) and local-charge phases. Even though the Hamiltonian exhibits different symmetries in the spin and charge sectors, the thermodynamic properties near the two types of quantum phase transition are closely related under spin-charge interchange. Moreover, the critical responses to a local magnetic field (for small impurity-boson coupling) and to an electric potential (for large impurity-boson coupling) are characterized by the same exponents, whose values place these quantum-critical points in the universality class of the pseudogap Anderson model. One specific case of the pseudogap Anderson-Holstein model may be realized in a double-quantum-dot device, where the quantum phase transitions manifest themselves in the finite-temperature linear electrical conductance.

DOI: 10.1103/PhysRevB.87.075145 PACS number(s): 71.10.Hf, 75.30.Hx, 72.10.Di, 64.60.ae

I. INTRODUCTION

Quantum phase transitions (QPTs) take place between competing ground states at the absolute zero of temperature ($T = 0$) upon variation of a nonthermal control parameter.[1,2] QPTs are thought to play a role in many important open problems in condensed-matter physics, including high-temperature superconductivity,[3–5] the phase diagram for magnetic heavy-fermion metals,[6,7] and various types of metal-insulator transition.[8,9]

An interesting class of zero-temperature transitions is impurity or boundary QPTs at which only a subset of system degrees of freedom becomes critical.[10] A well-studied example arises in the pseudogap Anderson impurity model[11–17] of an interacting impurity level hybridizing with a host density of states that vanishes in power-law fashion precisely at the Fermi energy, a property that can be realized in a number of systems including unconventional d-wave superconductors,[18] certain semiconductor heterostructures,[19] and a particular double-quantum-dot setup.[20–22] The reduction of the density of states near the Fermi energy leads to QPTs between strong-coupling (Kondo-screened) and local-moment phases.[11] At the transitions, the system exhibits a critical response to a local magnetic field applied only to the impurity site.[23–25]

Impurity quantum phase transitions have been predicted[20–22,26–32] and possibly observed[33,34] to arise in various nanodevices. While strong electron-electron interactions are an integral element of such nanodevices, experiments on single-molecule transistors[35] and quantum-dot cavities[36] have also highlighted the importance of electron-phonon interactions. The main aspects of the last two experiments appear to be captured by variants of the Anderson-Holstein model, which supplements the Anderson model[37] for a magnetic impurity in a metallic host with a Holstein coupling[38] of the impurity charge to a local bosonic mode, usually assumed to represent an optical phonon. The model has been studied since the 1970s in connection with the mixed-valence problem,[39–46] the role of negative-U centers in superconductors,[47,48] and, most recently, single-molecule devices.[50,51] Various analytical approximations as well as nonperturbative numerical renormalization-group calculations have shown that the Holstein coupling reduces the Coulomb repulsion between two electrons in the impurity level, even yielding effective electron-electron attraction for sufficiently strong impurity-boson coupling. Furthermore, for the full Anderson-Holstein model with nonzero hybridization, as the impurity-boson coupling increases from zero, there can be a crossover from a conventional Kondo effect, involving conduction-band screening of the impurity spin degree of freedom, to a "charge Kondo effect" in which it is the impurity "isospin" or deviation from half-filling that is quenched by the conduction band. However, the evolution between these limits is entirely smooth, and the model exhibits no QPT.

This paper reports the results of study of a pseudogap Anderson-Holstein model which incorporates the structured conduction-band density of states from the pseudogap Anderson model into the Anderson-Holstein model. The essential physics of the problem, revealed using a combination of poor-man's scaling and the numerical renormalization group (NRG), is shown to depend on the sign of the effective Coulomb interaction between two electrons in the impurity level, on the presence or absence of particle-hole (charge-conjugation) symmetry and time-reversal symmetry, and on the value of the exponent r characterizing the variation $\rho(\varepsilon) \propto |\varepsilon|^r$ of the density of states near the Fermi energy $\varepsilon = 0$. Even though the pseudogap Anderson-Holstein Hamiltonian has a lower symmetry than the pseudogap Anderson Hamiltonian, the universal properties of the former model, including the structure of the renormalization-group fixed points and the values of critical exponents describing properties in the vicinity of those fixed points, are identical to those of the latter model as generalized to allow for negative (attractive) as

well as positive values of the local interaction U between two electrons in the impurity level.[25] The pseudogap Anderson-Holstein model can therefore be regarded in part as providing a physically plausible route to accessing the negative-U regime of the pseudogap Anderson model. Anderson impurities with $U < 0$ have recently attracted attention as a possible route to achieving enhanced thermoelectric power.[52]

The remainder of this paper is organized as follows: Section II introduces the pseudogap Anderson-Holstein model, analyzes special cases in which the model reduces to problems that have been studied previously, outlines a perturbative scaling analysis of the full model, and summarizes the NRG approach used to provide nonperturbative solutions of the model. Section III presents results under conditions of particle-hole and time-reversal symmetry, while Sec. IV addresses the general model with band exponent r between 0 and 1. Section V focuses on the specific case $r = 2$ relevant to a boson-coupled double-quantum-dot device. Section VI summarizes the main results of the paper. The Appendix contains details of the perturbative scaling analysis.

II. MODEL HAMILTONIAN, PRELIMINARY ANALYSIS, AND SOLUTION METHOD

A. Pseudogap Anderson-Holstein model

In this work, we study the pseudogap Anderson-Holstein model described by the Hamiltonian

$$\hat{H} = \hat{H}_{\rm imp} + \hat{H}_{\rm band} + \hat{H}_{\rm boson} + \hat{H}_{\text{imp-band}} + \hat{H}_{\text{imp-boson}}, \tag{1}$$

where

$$\hat{H}_{\rm imp} = \delta_d\,(\hat{n}_d - 1) + \frac{1}{2}U(\hat{n}_d - 1)^2, \tag{2a}$$

$$\hat{H}_{\rm band} = \sum_{\mathbf{k},\sigma} \varepsilon_{\mathbf{k}} c^\dagger_{\mathbf{k}\sigma} c_{\mathbf{k}\sigma}, \tag{2b}$$

$$\hat{H}_{\rm boson} = \omega_0\, b^\dagger b, \tag{2c}$$

$$\hat{H}_{\text{imp-band}} = \frac{1}{\sqrt{N_k}} \sum_{\mathbf{k},\sigma} (V_{\mathbf{k}} d^\dagger_\sigma c_{\mathbf{k}\sigma} + \text{H.c.}), \tag{2d}$$

$$\hat{H}_{\text{imp-boson}} = \lambda(\hat{n}_d - 1)(b + b^\dagger). \tag{2e}$$

Here, d_σ annihilates an electron of spin z component $\sigma = \pm\frac{1}{2}$ (or $\sigma = \uparrow, \downarrow$) and energy $\varepsilon_d = \delta_d - \frac{1}{2}U < 0$ in the impurity level, $\hat{n}_d = \sum_\sigma \hat{n}_{d\sigma}$ (with $\hat{n}_{d\sigma} = d^\dagger_\sigma d_\sigma$) is the total impurity occupancy, and $U > 0$ is the Coulomb repulsion between two electrons in the impurity level.[53] $V_{\mathbf{k}}$ is the hybridization matrix element between the impurity and a conduction-band state of energy $\varepsilon_{\mathbf{k}}$ annihilated by fermionic operator $c_{\mathbf{k}\sigma}$, and λ characterizes the Holstein coupling of the impurity occupancy to the displacement of a local vibrational mode of frequency ω_0. N_k is the number of unit cells in the host metal and, hence, the number of inequivalent $\mathbf{k}$ values. Without loss of generality, we take $V_{\mathbf{k}}$ and λ to be real and non-negative. For compactness of notation, we drop all factors of the reduced Planck constant $\hbar$, Boltzmann's constant k_B, the impurity magnetic moment $g\mu_B$, and the electronic charge e.

The conduction-band dispersion $\varepsilon_{\mathbf{k}}$ and the hybridization $V_{\mathbf{k}}$ affect the impurity degrees of freedom only through the hybridization function[54]

$$\mathbf{\Gamma}(\varepsilon) \equiv \frac{\pi}{N_k} \sum_{\mathbf{k}} |V_{\mathbf{k}}|^2 \delta(\varepsilon - \varepsilon_{\mathbf{k}}). \tag{3}$$

To focus on the most interesting physics of the model, we assume a simplified form

$$\mathbf{\Gamma}(\varepsilon) = \Gamma\,|\varepsilon/D|^r\,\Theta(D - |\varepsilon|), \tag{4}$$

where $\Theta(x)$ is the Heaviside function and we refer to the prefactor Γ as the hybridization width. In this notation, the case $r = 0$ represents a conventional metallic hybridization function. This paper focuses on cases $r > 0$ in which the hybridization function exhibits a power-law pseudogap around the Fermi energy. One way that such a hybridization function can arise is from a purely local hybridization matrix element $V_{\mathbf{k}} = V$ combined with a density of states (per unit cell per spin orientation) varying as

$$\rho(\varepsilon) \equiv N_k^{-1} \sum_{\mathbf{k}} \delta(\varepsilon - \varepsilon_{\mathbf{k}}) = \rho_0 |\varepsilon/D|^r \Theta(D - |\varepsilon|), \tag{5}$$

in which case $\Gamma = \pi\rho_0 V^2$. However, the results presented in this paper apply equally to situations in which the $\mathbf{k}$ dependence of the hybridization contributes to the energy dependence of $\mathbf{\Gamma}(\varepsilon)$.

The assumption that $\mathbf{\Gamma}(\varepsilon)$ exhibits a pure power-law dependence over the entire width of the conduction band is a convenient idealization. More realistic hybridization functions in which the power-law variation is restricted to a region around the Fermi energy exhibit the same qualitative physics, with modification only of nonuniversal properties such as critical couplings and Kondo temperatures.

The properties of the Hamiltonian specified by Eqs. (1)–(4) turn out to depend crucially on whether or not the system is invariant under the particle-hole transformation $c_{\mathbf{k}\sigma} \to c^\dagger_{\mathbf{k}\sigma}$, $d_\sigma \to -d^\dagger_\sigma$, $b \to -b$, which maps $\varepsilon_{\mathbf{k}} \to -\varepsilon_{\mathbf{k}}$ and $\delta_d \to -\delta_d$. For the symmetric hybridization function given in Eq. (4), the condition for particle-hole symmetry is $\delta_d = 0$ corresponding to $\varepsilon_d = -\frac{1}{2}U$.

B. Review of related models

Before addressing the full pseudogap Anderson-Holstein model, it is useful to review two limiting cases that have been studied previously.

1. Pseudogap Anderson model

For coupling $\lambda = 0$, the pseudogap Anderson-Holstein model reduces to the pseudogap Anderson model[12–17,24,25] plus free local bosons. In the conventional ($r = 0$) Anderson impurity model, the generic low-temperature limit is a strong-coupling regime in which the impurity level is effectively absorbed into the conduction band.[55] In the pseudogapped ($r > 0$) variant of the model, the depression of the hybridization function around the Fermi energy gives rise to a competing local-moment phase in which the impurity retains an unscreened spin degree of freedom all the way to absolute zero. The $T = 0$ phase diagram of this model depends on the presence or absence of particle-hole symmetry[14] and of time-reversal symmetry.[25]

Behavior at particle-hole symmetry ($\delta_d = 0$). For any band exponent $0 < r < \frac{1}{2}$, in zero magnetic field there is a continuous QPT at a critical coupling $\Gamma = \Gamma_c(r,U,\delta_d = 0)$ between the local-moment phase and a symmetric strong-coupling phase. In the local-moment phase (reached for $0 \leqslant \Gamma < \Gamma_c$), the impurity contributions[56] to the entropy and to the static spin susceptibility approach the low-temperature limits $S_{\rm imp} = \ln 2$ and $T\chi_{s,\rm imp} = \frac{1}{4}$, respectively, while conduction electrons at the Fermi energy experience an s-wave phase shift $\delta_0(\varepsilon = 0) = 0$. In the symmetric strong-coupling phase ($\Gamma > \Gamma_c$), the corresponding properties are $S_{\rm imp} = 2r \ln 2$, $T\chi_{s,\rm imp} = r/8$, and $\delta_0(0) = -(1-r)(\pi/2)\,\mathrm{sgn}\,\varepsilon$, all indicative of partial quenching of the impurity degrees of freedom.

A magnetic field that couples to the band electrons moves the zero in the density of states of each spin species away from the Fermi level and washes out all pseudogap physics at energies below the Zeeman scale.[25] More interesting is the breaking of time-reversal symmetry by a local magnetic field that couples only to the impurity degree of freedom and enters the Anderson model through an additional Hamiltonian term

$$H_h = \frac{h}{2}(\hat{n}_{d\uparrow} - \hat{n}_{d\downarrow}). \tag{6}$$

The critical response to an infinitesimal h reveals that the transition between the local-moment and strong-coupling phases takes place at an interacting quantum-critical point.[23–25] However, a finite value of h destabilizes both the local-moment phase[25] and the symmetric strong-coupling phase,[57] and destroys the QPT between the two.[58] For any $h \neq 0$, the ground state of the particle-hole-symmetric model (with $U > 0$) is a fully polarized local moment that is asymptotically decoupled from the conduction band.[58]

For $r \geqslant \frac{1}{2}$, the symmetric strong-coupling fixed point is unstable even in zero magnetic field,[13,14] and a particle-hole-symmetric system lies in the local-moment phase for all values of Γ.

Behavior away from particle-hole symmetry ($\delta_d \neq 0$). In zero magnetic field, the model remains in the local-moment phase described above for all $|\delta_d| < \frac{1}{2}U$ (i.e., $-U < \varepsilon_d < 0$) and $\Gamma < \Gamma_c(r,U,\delta_d) \equiv \Gamma_c(r,U,-\delta_d)$. As shown schematically in Fig. 1, the critical hybridization width Γ_c increases monotonically from zero as $|\delta_d|$ drops below $\frac{1}{2}U$. For $0 < r < \frac{1}{2}$ [Fig. 1(a)], $\Gamma_c(r,U,\delta_d)$ smoothly approaches the symmetric critical value $\Gamma_c(r,U,0)$ as $\delta_d \to 0$. For $r \geqslant \frac{1}{2}$ [Fig. 1(b)], $\Gamma_c(r,U,\delta_d)$ instead diverges as $\delta_d \to 0$, consistent with the $\delta_d = 0$ behavior discussed above.

For $\delta_d \neq 0$ and $\Gamma > \Gamma_c$, the model lies in one of two asymmetric strong-coupling phases that share the low-temperature properties $S_{\rm imp} = 0$ and $T\chi_{s,\rm imp} = 0$. For $\delta_d > 0$, the Fermi-energy phase shift is $\delta_0(0) = -\pi\,\mathrm{sgn}\,\varepsilon$, while the ground-state charge (total fermion number measured from half-filling) is $Q = -1$. For $\delta_d < 0$, by contrast, $\delta_0(0) = +\pi\,\mathrm{sgn}\,\varepsilon$ and $Q = +1$. We label these two phases ASC_- and ASC_+ according to the sign of Q.

For $r < r^* \simeq \frac{3}{8}$, the low-temperature physics on the phase boundary $\Gamma = \Gamma_c(r,U,\delta_d \neq 0)$ is identical to that at $\Gamma = \Gamma_c(r,U,0)$, whereas for $r > r^*$ the properties are distinct.[14,25] For $r^* < r < 1$, the response to an infinitesimal local magnetic field shows that asymmetric transitions take place at two interacting quantum-critical points (one for $\delta_d > 0$, the other for $\delta_d < 0$). For $r \geqslant 1$, the QPTs are first order[23] and can be interpreted as renormalized level crossings between the local-moment doublet and the $\mathrm{ASC}_\pm$ singlet ground states.[25]

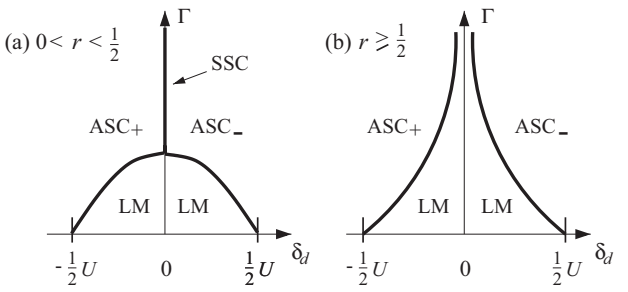

FIG. 1. Schematic δ_d-Γ phase diagrams of the pseudogap Anderson model [Eqs. (1)–(4) with $\lambda = 0$] for band exponents (a) $0 < r < \frac{1}{2}$, (b) $r \gtrsim \frac{1}{2}$. Generically, the system falls into either a local-moment phase (LM) or one of two asymmetric strong-coupling phases ($\mathrm{ASC}_\pm$). However, there is also a symmetric strong-coupling phase (the line labeled SSC) that is reached only for $0 < r < \frac{1}{2}$ under conditions of strict particle-hole symmetry ($\delta_d = 0$) and for sufficiently large hybridization widths Γ.

The asymmetric strong-coupling phase is stable over a range of local magnetic fields.[57] However, at a critical value of $|h|$ the system undergoes a level-crossing QPT into the same fully polarized phase as is found at particle-hole symmetry.[25]

Relationship to the pseudogap Kondo model. In cases where $\Gamma \ll \frac{1}{2}U - |\delta_d|$, the pseudogap Anderson model can be mapped via a Schrieffer-Wolff transformation[59] onto the pseudogap Kondo model.[11] The latter model exhibits QPTs entirely equivalent to those described above.[14] This allows us to identify critical exponents obtained previously for the pseudogap Kondo model[23] as the values that apply to the special case $\lambda = 0$ of the pseudogap Anderson-Holstein model.

2. Anderson-Holstein model

For $r = 0$, the pseudogap Anderson-Holstein model reduces to the Anderson-Holstein model.[39–51] Insight into the physics of both models can be gained by performing a canonical transformation of the Lang-Firsov type[60] to eliminate the Holstein coupling between the bosons and the impurity occupancy [Eq. (2e)]. The transformation[43]

$$\bar{H} = e^S \hat{H} e^{-S} \quad \text{with} \quad S = \frac{\lambda}{\omega_0}(\hat{n}_d - 1)(b^\dagger - b) \tag{7}$$

maps Eq. (1) to

$$\bar{H} = \bar{H}_{\rm imp} + \hat{H}_{\rm band} + \hat{H}_{\rm boson} + \bar{H}_{\rm imp\text{-}band}, \tag{8}$$

in which $\hat{H}_{\rm boson}$ and $\hat{H}_{\rm band}$ remain as given in Eqs. (2c) and (2b), respectively. $\bar{H}_{\rm imp}$ is identical to $\hat{H}_{\rm imp}$ [Eq. (2a)] apart from the replacement of U by

$$\bar{U} = U - 2\varepsilon_p, \tag{9}$$

where the polaron energy

$$\varepsilon_p = \lambda^2/\omega_0 \tag{10}$$

represents an important energy scale in the problem. The invariance of δ_d under the mapping implies a renormalization of the level energy from $\varepsilon_d = \delta_d - \frac{1}{2}U$ to

$$\bar{\varepsilon}_d = \varepsilon_d + \varepsilon_p. \tag{11}$$

Finally, the impurity-band coupling term becomes

$$\bar{H}_{\text{imp-band}} = \frac{1}{\sqrt{N_s}} \sum_{\mathbf{k},\sigma} V_{\mathbf{k}} (B^\dagger d_\sigma^\dagger c_{\mathbf{k}\sigma} + \text{H.c}), \tag{12}$$

with

$$B = e^{-(\lambda/\omega_0)(b^\dagger - b)}. \tag{13}$$

The canonical transformation in Eq. (7) maps the local boson mode to

$$\bar{b} = e^S b\, e^{-S} = b - (\lambda/\omega_0)(\hat{n}_d - 1), \tag{14}$$

effectively defining a different displaced-oscillator basis for each value of the impurity occupancy n_d, namely, the basis that minimizes the ground-state energy of $\hat{H}_{\text{imp}} + \hat{H}_{\text{boson}} + \hat{H}_{\text{imp-boson}}$. The elimination of the Holstein coupling is accompanied by two compensating changes to the Hamiltonian: a reduction in the magnitude (or even a change in the sign) of the interaction within the impurity level, reflecting the fact that Eq. (2e) lowers the energy of the empty and doubly occupied impurity configurations relative to single occupation; and incorporation into the impurity-band term [Eq. (12)] of operators B and $B^\dagger$ that cause each hybridization event to be accompanied by the creation and absorption of a packet of bosons as the local mode adjusts to the change in the impurity occupancy n_d.

The analysis of Eq. (8) is trivial in the case $\Gamma = 0$ of zero hybridization where the Fock space can be partitioned into subspaces of fixed impurity occupancy $n_d = 0$, 1, and 2, and the ground state within each sector corresponds to the vacuum of the transformed boson mode. It can be seen from Eq. (9) that the effective onsite Coulomb interaction changes sign at $\lambda = \lambda_0$, where

$$\lambda_0 = \sqrt{\omega_0 U/2}\,. \tag{15}$$

For weak bosonic couplings $\lambda < \lambda_0$, the effective interaction is repulsive, and for $|\delta_d| < \frac{1}{2}\bar{U}$ the impurity ground state is a spin doublet with $n_d = 1$ and $\sigma = \pm\frac{1}{2}$. For $\lambda > \lambda_0$, by contrast, the strong coupling to the bosonic mode yields an attractive effective onsite interaction and for $|\delta_d| < -\frac{1}{2}\bar{U}$ the two lowest-energy impurity states are spinless but have a charge (relative to half-filling) $Q = n_d - 1 = \pm 1$; these states are degenerate only under conditions of strict particle-hole symmetry ($\delta_d = 0$).

Various limiting behaviors of the full Anderson-Holstein model with $\Gamma \neq 0$ are understood:[43,49]

(i) If ω_0 and λ are both taken to infinity in such a way that ε_p defined in Eq. (10) approaches a finite value, the model behaves just like the pure-fermionic Anderson model with U replaced by $\bar{U}$, while Γ and δ_d are unaffected by the bosonic coupling (implying that $\varepsilon_d = \delta_d - \frac{1}{2}U$ is replaced by $\bar{\varepsilon}_d$).

(ii) In the *instantaneous* or *antiadiabatic* limit $\Gamma \ll \omega_0 < \infty$, the bosons adjust rapidly to any change in the impurity occupancy; for $\omega_0, U \gg \varepsilon_p$, the physics essentially remains that of the Anderson model with $U \to \bar{U}$, while for $\omega_0, U \ll \varepsilon_p$, there is also a reduction from Γ to $\Gamma_{\text{eff}} = \Gamma \exp(-\varepsilon_p/\omega_0)$ in the hybridization width describing scattering between the $n_d = 0$ and 2 sectors, reflecting the reduced overlap between the ground states in these two sectors.

(iii) In the *adiabatic* limit $\Gamma \gg \omega_0$, by contrast, the bosons are unable to adjust on the typical time scale of hybridization events, and neither U nor Γ undergoes significant renormalization.

(iv) In the physically most relevant regime $\Gamma \lesssim \omega_0 < U, D$, NRG calculations[43,50] show that for $\Gamma \ll |\delta_d| \ll U$, there is a smooth crossover from a conventional charge-sector Kondo effect for $\lambda \ll \lambda_0$ (and thus $\Gamma \ll \bar{U}$) to a charge-sector analog of the Kondo effect for $\lambda \gg \lambda_0$ (and $\Gamma \ll -\bar{U}$). The primary goal of this work is to explain how this physics is modified by the presence of a pseudogap in the impurity hybridization function.

C. Poor-man's scaling

As a preliminary step in the analysis of the pseudogap Anderson-Holstein Hamiltonian, we develop poor-man's scaling equations describing the evolution of model parameters under progressive reduction of the conduction bandwidth. Haldane's scaling analysis[61] of the metallic ($r = 0$) Anderson model in the limit $U \gg D$ has previously been extended to the pseudogap case $r > 0$, both for infinite[12] and finite[62] onsite interactions U. Here, the analysis is further generalized to treat the antiadiabatic regime of the Anderson-Holstein model with both metallic and pseudogapped densities of states.

Our analysis begins with the Lang-Firsov canonical transformation (7). In the antiadiabatic regime, it is a good approximation to calculate all physical properties in the vacuum state of the transformed boson mode defined in Eq. (14). We therefore focus on many-body states representing the direct product of the bosonic vacuum with the half-filled Fermi sea and with one of the four possible configurations of the impurity level. In the atomic limit $\Gamma = 0$, the energies of the states having impurity occupancy $n_d = 0$, 1, and 2 can be denoted E_0, $E_1 = E_0 + \bar{\varepsilon}_d$, and $E_2 = E_1 + \bar{\varepsilon}_d + \bar{U} = 2E_1 - E_0 + \bar{U}$, respectively.

The poor-man's scaling procedure involves progressive reduction of the conduction-band halfwidth from D to $\tilde{D}$. At each infinitesimal step $\tilde{D} \to \tilde{D} + d\tilde{D} < \tilde{D}$, the energies E_0, E_1, and E_2, as well as the hybridization function Γ are adjusted to compensate for the elimination of virtual hybridization processes involving band states in the energy windows $\tilde{D} + d\tilde{D} < \varepsilon < \tilde{D}$ and $-\tilde{D} < \varepsilon < -(\tilde{D} + d\tilde{D})$. An added complication in the Anderson-Holstein model is the presence of the operators B and $B^\dagger$ in Eq. (12), which allow virtual excitation of states having arbitrarily high boson occupation numbers $\bar{n}_b = \bar{b}^\dagger \bar{b}$. As detailed in the Appendix, summation over all such intermediate states leads to the scaling equations

$$\frac{d\tilde{U}}{d\tilde{D}} = \frac{2\tilde{\Gamma}}{\pi}\left[\frac{1}{\mathcal{E}(\tilde{D} + \tilde{\varepsilon}_d)} - \frac{1}{\mathcal{E}(\tilde{D} - \tilde{\varepsilon}_d)} + \frac{1}{\mathcal{E}(\tilde{D} - \tilde{U} - \tilde{\varepsilon}_d)} - \frac{1}{\mathcal{E}(\tilde{D} + \tilde{U} + \tilde{\varepsilon}_d)}\right], \tag{16}$$

$$\frac{d\tilde{\varepsilon}_d}{d\tilde{D}} = \frac{\tilde{\Gamma}}{\pi}\left[\frac{1}{\mathcal{E}(\tilde{D}-\tilde{\varepsilon}_d)} - \frac{2}{\mathcal{E}(\tilde{D}+\tilde{\varepsilon}_d)} + \frac{1}{\mathcal{E}(\tilde{D}+\tilde{U}+\tilde{\varepsilon}_d)}\right], \tag{17}$$

$$\frac{d\tilde{\Gamma}}{d\tilde{D}} = r\,\frac{\tilde{\Gamma}}{\tilde{D}} \tag{18}$$

for renormalized model parameters that take bare values $\tilde{U} = \bar{U}$ [Eq. (9)], $\tilde{\varepsilon}_d = \bar{\varepsilon}_d$ [Eq. (11)], and $\tilde{\Gamma} = \Gamma$ for $\tilde{D} = D$. In these equations, the energy scale

$$\mathcal{E}(E) = E \Big/ S\left(\frac{E}{\omega_0}, \frac{\varepsilon_p}{\omega_0}\right) \tag{19}$$

is defined in terms of a dimensionless function

$$S(a,x) = a\,e^{-|x|}\sum_{n=0}^{\infty}\frac{1}{n!}\,\frac{x^n}{a+n} \equiv a\,\Gamma(a)\,\gamma^*(a,-x)\,e^{-|x|}, \tag{20}$$

where $\Gamma(a)$ is the gamma function and $\gamma^*(a,x)$ is related to the lower incomplete gamma function.[63]

In the case $\lambda = 0$ where $\mathcal{E}(E) = E$, Eqs. (16)–(18) reduce to the scaling equations for the pseudogap Anderson model.[62] The pseudogap in the hybridization function produces a strong downward rescaling of $\tilde{\Gamma}$ [see Eq. (18)] that leads, via Eqs. (16) and (17), to weaker renormalization of $\tilde{U}$ and $\tilde{\varepsilon}_d$ than would occur in a metallic ($r = 0$) host. For $\lambda > 0$, one finds that $|\mathcal{E}(E)| > |E|$, so the bosonic coupling acts to further reduce (in magnitude) the right-hand sides of Eqs. (16) and (17), and produces still slower renormalization of $\tilde{U}$ and $\tilde{\varepsilon}_d$ with decreasing $\tilde{D}$. It should be noted that neither the bosonic energy ω_0 nor the electron-boson coupling λ is renormalized under the scaling procedure, and that the scaling equations respect particle-hole symmetry in that bare couplings satisfying $\varepsilon_d = -\frac{1}{2}U$ inevitably lead to rescaled couplings that satisfy $\tilde{\varepsilon}_d = -\frac{1}{2}\tilde{U}$.

Equation (18) can readily be solved to give

$$\tilde{\Gamma}(\tilde{D}) = (\tilde{D}/D)^r\,\Gamma. \tag{21}$$

For $\lambda > 0$, it is not possible to integrate Eqs. (16) and (17) in closed form due to the presence of the nontrivial function $\mathcal{E}(E)$ on their right-hand sides. The equations have been derived only to lowest order in nondegenerate perturbation theory, and are therefore limited in validity to the range $|\tilde{U}|, |\tilde{\varepsilon}_d|, \tilde{\Gamma} \ll \tilde{D}$. Nonetheless, one may be able to obtain useful insight into the qualitative physics of the model through numerical integration of Eqs. (16) and (17) until one of the following conditions is met, implying entry into a low-energy regime governed by a simpler effective model than the full pseudogap Anderson-Holstein model:

(i) If $\tilde{\varepsilon}_d, \tilde{U}+2\tilde{\varepsilon}_d > \tilde{D} > \tilde{\Gamma}$, the system should enter the empty-impurity region of the strong-coupling phase, where the impurity degree of freedom is frozen with an occupancy close to zero.

(ii) If $-(\tilde{U}+\tilde{\varepsilon}_d), -(\tilde{U}+2\tilde{\varepsilon}_d) > \tilde{D} > \tilde{\Gamma}$, the system should enter the full-impurity region of the strong-coupling phase, where the impurity degree of freedom is frozen with an occupancy close to two.

(iii) If $-\tilde{\varepsilon}_d, \tilde{U}+\tilde{\varepsilon}_d > \tilde{D} > \tilde{\Gamma}$, the system is expected to enter an intermediate-energy local-moment regime in which the impurity states with $n_d \neq 1$ are frozen out. As discussed further in Sec. III B, one can perform a generalization of the Schrieffer-Wolff transformation[59] to map the pseudogap Anderson-Holstein model to a pseudogap Kondo model with the density of states in Eq. (5). Depending on the value of the Kondo exchange coupling generated by the Schrieffer-Wolff transformation, the system may lie either in the strong-coupling phase of the pseudogap Kondo model (which should correspond to another region of the strong-coupling phase of the Anderson-Holstein model) or in a local-moment phase where the impurity retains a free twofold spin degree of freedom down to absolute zero.

(iv) If $\tilde{\varepsilon}_d, -(\tilde{U}+\tilde{\varepsilon}_d) > \tilde{D} > \tilde{\Gamma}, \tilde{U}+2\tilde{\varepsilon}_d$, the system should enter an intermediate-energy local-charge regime in which the $n_d = 1$ impurity states become frozen out. A generalized Schrieffer-Wolff transformation can map the pseudogap Anderson-Holstein model to a pseudogap charge Kondo model (see Sec. III B). The system may lie either in the strong-coupling phase of the charge Kondo model (yet another region of the strong-coupling phase of the Anderson-Holstein model) or in a local-charge phase of both models (where the impurity retains a free twofold charge degree of freedom down to absolute zero).

(v) If $\tilde{\Gamma} > \tilde{D} > |\tilde{\varepsilon}_d|$ and/or $\tilde{\Gamma} > \tilde{D} > |\tilde{U}+\tilde{\varepsilon}_d|$, then the system should enter the mixed-valence region of the strong-coupling phase.

Since each of the crossovers described above lies beyond the range of validity of the scaling equations, the preceding analysis is only suggestive. In order to provide a definitive account of the pseudogap Anderson-Holstein model, it is necessary to obtain full, nonperturbative solutions, such as those provided by the numerical renormalization group. However, we shall return to the scaling equations in Sec. V B to assist in the quantitative analysis of numerical results.

D. Numerical solution method

We have solved the model Eq. (1) using the numerical renormalization-group (NRG) method,[55,64,65] as extended to treat problems with an energy-dependent hybridization function,[13,14] and ones that involve local bosons.[43] Briefly, the procedure involves three key steps: (i) Division of the full range of conduction-band energies $-D \leqslant \varepsilon_{\mathbf{k}} \leqslant D$ into a set of logarithmic intervals bounded by $\varepsilon_m = \pm D\Lambda^{-m}$ for $m = 0,1,2,\ldots,$ where $\Lambda > 1$ is the Wilson discretization parameter. The continuum of states within each interval is replaced by a single state of each spin σ, namely, the linear combination of states lying within the interval that couples to the impurity. (ii) Application of the Lanczos procedure to map the discretized version of $\hat{H}_{\rm band}$ onto a tight-binding form[66]

$$\hat{H}_{\rm band} = \sum_{n=0}^{\infty}\Lambda^{-n/2}\,t_n\sum_{\sigma}(f_{n\sigma}^{\dagger}f_{n-1,\sigma} + \text{H.c.}), \tag{22}$$

where $f_{0\sigma} \propto \sum_{\mathbf{k}} V_{\mathbf{k}} c_{\mathbf{k}\sigma}$, and $\{f_{n,\sigma}, f_{n',\sigma'}^{\dagger}\} = \delta_{n,n'}\,\delta_{\sigma,\sigma'}$. The hopping parameters t_n (with $t_0 = 0$) contain all information about the energy dependence of the hybridization function $\mathbf{\Gamma}(\varepsilon)$. (iii) Iterative solution of the problem via diagonalization

of a sequence of rescaled Hamiltonians

$$\hat{H}_0 = \hat{H}_{\rm imp} + \hat{H}_{\rm boson} + \hat{H}_{\rm imp\text{-}band} + \hat{H}_{\rm imp\text{-}boson} - E_{G,0} \tag{23}$$

and

$$\hat{H}_N = \sqrt{\Lambda}\hat{H}_{N-1} + t_N \sum_\sigma (f^\dagger_{N\sigma} f_{N-1,\sigma} + \text{H.c.}) - E_{G,N} \tag{24}$$

for $N = 1, 2, 3, \ldots$, where $E_{G,N}$ is chosen so that the ground-state energy of $\hat{H}_N$ is zero. $\hat{H}_N$ can be interpreted as describing a fermionic chain of length $N+1$ sites with hopping coefficients that decay exponentially along the chain away from the end (site $n = 0$) to which the impurity and bosonic degrees of freedom couple. The solution of $\hat{H}_N$ captures the dominant physics at energies and temperatures of order $D\Lambda^{-N/2}$.

The NRG procedure is iterated until the problem reaches a fixed point at which the spectrum of $\hat{H}_N$ and the matrix elements of all physical operators between the eigenstates are identical to those of $\hat{H}_{N-2}$. (The eigensolution of $\hat{H}_N$ differs from that of $\hat{H}_{N-1}$ even at a fixed point due to odd-even alternation effects.[55]) In addition to the conduction-band discretization, two further approximations must be imposed. First, the number of states on the fermionic chain grows by a factor of 4 at each iteration, making it impractical to keep track of all the many-body states beyond the first few iterations. Instead, one retains just the N_s many-particle states of lowest energy after iteration N, creating a basis of dimension $4N_s$ for iteration $N+1$. Second, the presence of local bosons adds the further complication that the full Fock space is infinite dimensional even at iteration $N = 0$, making it necessary to restrict the maximum number of bosons to some finite number N_b.

The NRG calculations reported in the sections that follow took advantage of the conserved eigenvalues of the total spin-z operator

$$\hat{S}_z = \frac{1}{2}(d^\dagger_\uparrow d_\uparrow - d^\dagger_\downarrow d_\downarrow) + \frac{1}{2}\sum_{n=0}^{N}(f^\dagger_{n\uparrow} f_{n\uparrow} - f^\dagger_{n\downarrow} f_{n\downarrow}), \tag{25}$$

and the total "charge" operator

$$\hat{Q} = \hat{n}_d - 1 + \sum_{n=0}^{N}(f^\dagger_{n\uparrow} f_{n\uparrow} + f^\dagger_{n\downarrow} f_{n\downarrow} - 1) \tag{26}$$

to reduce the Hamiltonian matrix to block-diagonal form, thereby reducing the labor of matrix diagonalization. In the absence of a magnetic field, the Hamiltonian $\hat{H}_N$ commutes not only with $\hat{S}_z$, but also with the total spin-raising and -lowering operators

$$\hat{S}_+ = d^\dagger_\uparrow d_\downarrow + \sum_n f^\dagger_{n\uparrow} f_{n\downarrow} \quad \text{and} \quad \hat{S}_- = (\hat{S}_+)^\dagger, \tag{27}$$

the other two generators of SU(2) spin symmetry. By analogy, one can interpret

$$\hat{I}_z = \frac{1}{2}\hat{Q}, \quad \hat{I}_+ = -d^\dagger_\uparrow d^\dagger_\downarrow + \sum_n (-1)^n f^\dagger_{n\uparrow} f^\dagger_{n\downarrow} \equiv (\hat{I}_-)^\dagger \tag{28}$$

as the generators of an SU(2) isospin symmetry. Since $[\hat{H}_{\rm imp\text{-}boson}, \hat{I}_\pm] \neq 0$, $\hat{H}_N$ does not exhibit full isospin rotation invariance, even though this symmetry turns out to be recovered in the asymptotic low-energy behavior at each of the important renormalization-group fixed points. In order to treat spin and charge degrees of freedom on equal footing, we elected not to exploit total spin conservation in our NRG calculations. However, in the sections that follow we identify NRG states by their quantum number S wherever appropriate.

Throughout the remainder of this paper, all energies are expressed as multiples of the half-bandwidth $D = 1$. Results are reported for the representative case of a strongly correlated impurity level having $U = 0.5$ coupled to a local bosonic mode of frequency $\omega_0 = 0.1$. The NRG calculations were performed using discretization parameter $\Lambda = 2.5$ or 3, allowing up to $N_b = 40$ bosons, values found to yield well-converged results for the model parameters considered. The number of retained many-body states was chosen sufficiently large to eliminate discernible truncation errors in each computed quantity; unless otherwise noted, this goal was attained using $N_s = 500$.

III. RESULTS: PARTICLE-HOLE-SYMMETRIC MODEL WITH BAND EXPONENT $0 < r < \frac{1}{2}$

As reviewed in Sec. II B, the particle-hole-symmetric pseudogap Anderson model with a band exponent $0 < r < \frac{1}{2}$ has a QPT at $\Gamma = \Gamma_c(r,U)$ between local-moment and symmetric strong-coupling phases. In this section, we investigate the changes that arise from the Holstein coupling of the impurity charge to a local boson mode. For bosonic couplings $\lambda < \lambda_0$ [see Eq. (15)], we find that the low-energy physics of the pseudogap Anderson-Holstein model is largely the same as for the pseudogap Anderson model with U replaced by an effective value $U_{\rm eff}$ [defined in Eq. (33) below] that differs from $\bar{U}$ introduced in Sec. II B2. A QPT at $\Gamma = \Gamma_{c1}(r,U,\lambda < \lambda_0) \simeq \Gamma_c(r,U_{\rm eff})$ exhibits universal properties indistinguishable from those at the critical point of the pseudogap Anderson model. For stronger bosonic couplings $\lambda > \lambda_0$, there is instead a QPT at $\Gamma = \Gamma_{c2}(r,U,\lambda > \lambda_0)$ between the symmetric strong-coupling phase and a local-charge phase in which the impurity has a residual twofold charge degree of freedom. The critical exponents describing the local-charge response at $\Gamma = \Gamma_{c2}$ are identical to those characterizing the local-spin response at $\Gamma = \Gamma_{c1}$.

All numerical results presented in this section were obtained in a zero or infinitesimal magnetic field for a symmetric impurity with $\varepsilon_d = -\frac{1}{2}U = -0.25$, for a bosonic frequency $\omega_0 = 0.1$, and for NRG discretization parameter $\Lambda = 3$.

A. NRG spectrum and fixed points

The first evidence for the existence of multiple phases of the symmetric pseudogap Anderson-Holstein model comes from the eigenspectrum of $\hat{H}_N$. This spectrum can be used to identify stable and unstable renormalization-group fixed points of the model.

1. Weak bosonic coupling

Figure 2(a) shows, for $r = 0.4$, $\lambda = 0.05 < \lambda_0 \simeq 0.158$, and seven different values of Γ, the variation with even

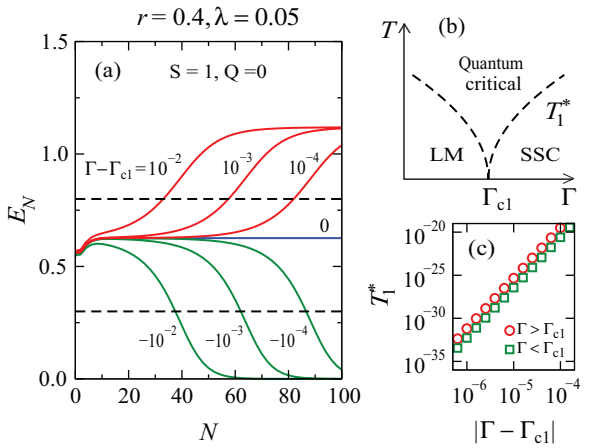

FIG. 2. (Color online) Particle-hole-symmetric pseudogap Anderson-Holstein model near its spin-sector critical point C_S: (a) NRG energy E_N vs even iteration number N of the first excited multiplet having quantum numbers $S = 1$, $Q = 0$, calculated for $r = 0.4$, $U = -2\varepsilon_d = 0.5$, $\omega_0 = 0.1$, $\lambda = 0.05 < \lambda_0 \simeq 0.158$, and seven values of $\Gamma - \Gamma_{c1}$ (with $\Gamma_{c1} \simeq 0.316\,680\,5$) labeled on the plot. (b) Schematic phase diagram on the Γ-T plane for $\lambda < \lambda_0$, showing the $T = 0$ transition between the local-moment ($\Gamma < \Gamma_{c1}$) and symmetric strong-coupling ($\Gamma > \Gamma_{c1}$) phases. Dashed lines mark the scale T_1^* of the crossover from the intermediate-temperature quantum-critical regime to one or other of the stable phases. (c) Crossover scale $T_1^* = D\Lambda^{-N_1^*/2}$ vs $|\Gamma - \Gamma_{c1}|$ in the local-moment and symmetric strong-coupling phases, showing the power-law behavior described in Eq. (38). Here, N_1^* is the interpolated value of N at which E_N in (a) leaves its quantum-critical range by crossing one or other of the horizontal dashed lines.

iteration number N of the energy of the first excited multiplet having quantum numbers $S = 1$, $Q = 0$. For small values of Γ, this energy E_N at first rises with increasing N, but eventually falls towards the value $E_{\rm LM} = 0$ expected at the *local-moment* fixed point corresponding to effective model couplings $\Gamma = \lambda = 0$ and $U = \infty$. At this fixed point, the impurity $n_d = 1$ doublet asymptotically decouples from the tight-binding chain of length $N + 1$, leaving a localized spin-$\frac{1}{2}$ degree of freedom and low-lying many-body excitations characterized by a Fermi-energy s-wave phase shift $\delta_0(\epsilon = 0) = 0$, identical to that at the local-moment fixed point of the pseudogap Anderson model (see Sec. II B2).

For large Γ, E_N instead rises monotonically to reach a limiting value $E_{\rm SSC} \simeq 1.119$ characteristic of the *symmetric strong-coupling* fixed point, corresponding to effective couplings $\Gamma = \infty$ and $U = \lambda = 0$. Here, the impurity level forms a spin singlet with an electron on the end ($n = 0$) site of the tight-binding chain. The singlet formation "freezes out" the end site, leaving free-fermionic excitations on a chain of reduced length N, leading to a Fermi-energy phase shift $\delta_0(0) = -(1 - r)(\pi/2)\,\mathrm{sgn}\,\varepsilon$. This is the same phase shift as is found at the symmetric strong-coupling fixed point of the pseudogap Anderson model.[14]

The local-moment and symmetric strong-coupling fixed points describe the large-N (low-energy $D\Lambda^{-N/2}$) physics for all initial choices of the hybridization width except $\Gamma = \Gamma_{c1} \simeq 0.316\,680\,5$, in which special case E_N rapidly approaches $E_c \simeq 0.6258$ and remains at that energy up to arbitrarily large N. This behavior can be associated with an unstable *critical point* C_S separating the local-moment and symmetric strong-coupling phases. (The subscript "S" indicates that C_S separates phases having different ground-state spin quantum numbers.) The critical point corresponds to the pseudogap Anderson-Holstein model with $\lambda = 0$ and Γ/U equaling some r-dependent critical value.

Whereas the critical coupling Γ_{c1} is a nonuniversal function of all the other model parameters (r, U, ω_0, and λ), the low-energy NRG spectra at the local-moment, symmetric strong coupling, and C_S fixed points depend only on the band exponent r and the NRG discretization parameter Λ. For given r and Λ, each spectrum is found to be identical to that at the corresponding fixed point of the particle-hole-symmetric pseudogap Anderson model. Not only can the spectrum be interpreted as arising from an effective boson coupling $\lambda = 0$, but it exhibits the SU(2) isospin symmetry that is broken in the full pseudogap Anderson-Holstein model.

2. Strong bosonic coupling

Figure 3(a) plots the energy at even iterations of the first NRG excited state having quantum numbers $S = Q = 0$ for $r = 0.4$, $\lambda = 0.2 > \lambda_0 \simeq 0.158$, and seven different Γ values. For $\Gamma > \Gamma_{c2} \simeq 0.687\,895\,6$, E_N eventually flows to the value $E_{\rm SSC} \simeq 1.119$ identified in the weak-bosonic-coupling regime, and examination of the full NRG spectrum confirms that the low-temperature behavior is governed by the same symmetric strong-coupling fixed point.

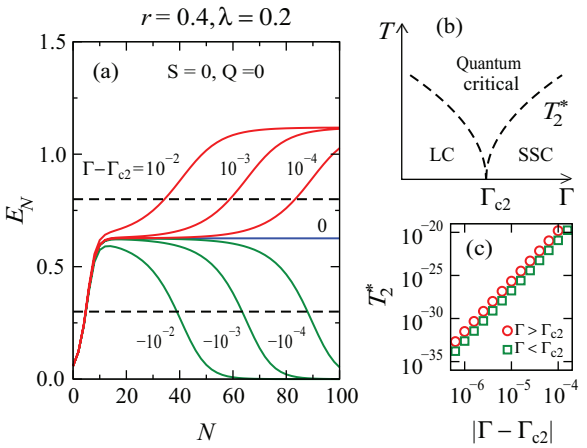

FIG. 3. (Color online) Particle-hole-symmetric pseudogap Anderson-Holstein model near its charge-sector critical point C_C: (a) NRG energy E_N vs even iteration number N of the first excited state having quantum numbers $S = Q = 0$, calculated for $r = 0.4$, $U = -2\varepsilon_d = 0.5$, $\omega_0 = 0.1$, $\lambda = 0.2 > \lambda_0 \simeq 0.158$, and seven values of $\Gamma - \Gamma_{c2}$ (with $\Gamma_{c2} \simeq 0.687\,895\,6$) labeled on the plot. (b) Schematic Γ-T phase diagram for $\lambda > \lambda_0$, showing the $T = 0$ transition between the local-charge and symmetric strong-coupling phases and the scale T_2^* of the crossover from the quantum-critical regime to a stable phase. (c) Crossover scale $T_2^* = D\Lambda^{-N_2^*/2}$ vs $|\Gamma - \Gamma_{c2}|$ in the local-charge and symmetric strong-coupling phases, showing the power-law behavior described in Eq. (39). Here, N_2^* is the interpolated value of N at which E_N in (a) leaves its quantum-critical range by crossing one or other of the horizontal dashed lines.

For $\Gamma < \Gamma_{c2}$, E_N flows to zero, the value found at the local-moment fixed point. In fact, all the fixed-point many-body states obtained for $\lambda > \lambda_0$ turn out to have the same energies as states at the local-moment fixed point. However, the quantum numbers of states in the $\lambda > \lambda_0$ spectrum and the local-moment spectra are not identical, but rather are related by the interchanges $S \leftrightarrow I$ and $S_z \leftrightarrow I_z$. We therefore associate the $\lambda > \lambda_0$ spectrum with a *local-charge* fixed point, corresponding to $\Gamma = \lambda = 0$ and $U = -\infty$, at which the impurity has a residual isospin-$\frac{1}{2}$ degree of freedom. Like its local-moment counterpart, this fixed point exhibits a phase shift $\delta_0(0) = 0$.

For $\Gamma = \Gamma_{c2}$, E_N rapidly approaches and remains at the same critical value E_c as found for $\lambda < \lambda_0$ and $\Gamma = \Gamma_{c1}$. Once again, however, the many-body spectrum is related to that at the corresponding weak-bosonic-coupling fixed point by interchange of spin and isospin quantum numbers, leading to the interpretation of this fixed point as a charge analog C_C of the critical point of the particle-hole-symmetric pseudogap Anderson model.

B. Phase boundaries

Figure 4 shows phase boundaries for the symmetric pseudogap Anderson-Holstein model, as established for $U = -2\varepsilon_d = 0.5$ and $\omega_0 = 0.1$ by examination of the NRG spectrum. In the atomic limit $\Gamma = 0$, we find a level-crossing transition between the local-moment and local-charge phases at $\lambda = \lambda_0 \simeq 0.15812(1)$, a value in excellent agreement with the prediction of Eq. (15). (Throughout this paper, a digit in parentheses following a number indicates the estimated nonsystematic error in the last digit of the number.) For each of four values of the band exponent r, the figure plots the critical hybridization widths Γ_{c1} (open symbols, for $0 \leqslant \lambda < \lambda_0$) and

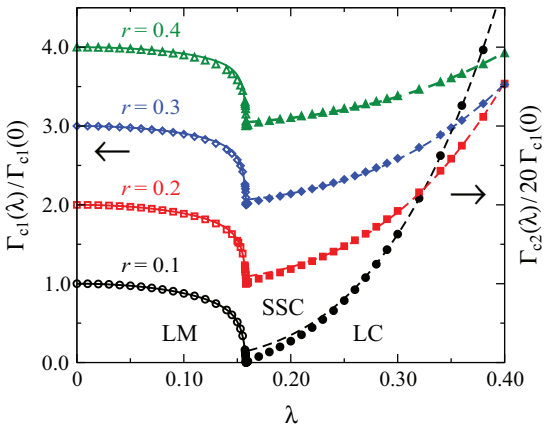

FIG. 4. (Color online) Phase boundaries of the particle-hole-symmetric pseudogap Anderson-Holstein model in zero magnetic field: variation with bosonic coupling λ of the critical hybridization widths Γ_{c1} and Γ_{c2}. Data for $U = -2\varepsilon_d = 0.5$, $\omega_0 = 0.1$, and band exponents $r = 0.1$, 0.2, 0.3, and 0.4 are scaled and offset for clarity: the quantities plotted are $\Gamma_{c1}(\lambda)/\Gamma_{c1}(0) + 10r - 1$ (empty symbols) and $\Gamma_{c2}(\lambda)/20\Gamma_{c1}(0) + 10r - 1$ (filled symbols). Solid lines show the prediction of Eq. (34), while dashed lines plot the form $A(r)\lambda^{2(2-r)}$ suggested by Eq. (37) with a prefactor $A(r)$ determined by fitting values of Γ_{c2} for $0.3 \leqslant \lambda \leqslant 0.4$.

Γ_{c2} (filled symbols, for $\lambda > \lambda_0$) normalized by the $\lambda = 0$ value of Γ_{c1}, which coincides with the critical hybridization width Γ_c of the corresponding pseudogap Anderson model. The lines represent analytical expressions for the phase boundaries that will be explained in the remainder of this section.

In the particle-hole-symmetric pseudogap Anderson model, the critical hybridization width $\Gamma_c(r,U)$ can be established by performing a Schrieffer-Wolff transformation[59] that maps the problem to a pseudogap Kondo model with a Kondo exchange coupling

$$\rho_0 J = \frac{8\Gamma}{\pi U}\left(\frac{U}{2D}\right)^r. \tag{29}$$

Here, the Kondo coupling in a conventional metal ($r = 0$) is multiplied by a factor $(U/2D)^r$ that accounts for the irrelevance of the hybridization width under poor-man's scaling [see Eq. (18)] while neglecting the much weaker renormalization of the onsite interaction [Eq. (16)]. The critical coupling J_c of the particle-hole-symmetric pseudogap Kondo model satisfies $\rho_0 J_c = j_c(r)$, where $j_c(r) \simeq r$ for $r \ll \frac{1}{2}$ (Ref. 11) and $j_c(r) \to \infty$ for $r \to \frac{1}{2}$ (Refs. 67, 14, and 15). Combining this condition with Eq. (29) yields

$$\Gamma_c = \frac{\pi}{4} j_c(r)\, D \left(\frac{U}{2D}\right)^{1-r}. \tag{30}$$

It is important to note that an equivalent expression has been derived within the local-moment approach to the pseudogap Anderson model without reference to a Schrieffer-Wolff transformation [see Eq. (6.10b) of Ref. 15] and has been verified via NRG calculations.[16] As such, Eq. (30) with a suitably chosen value of $j_c(r)$ is applicable even for r approaching $\frac{1}{2}$ where charge fluctuations for $\Gamma \simeq \Gamma_c$ are too strong to allow mapping to a Kondo model.[14] We now consider how Eq. (30) should be modified to describe the phase boundaries of the pseudogap Anderson-Holstein model.

1. Weak bosonic coupling

For $\lambda \ll \lambda_0$ (and hence $\bar{U} > 0$), it has been shown[50] that a generalized Schrieffer-Wolff transformation maps the particle-hole-symmetric Anderson-Holstein model to a Kondo model with a dimensionless exchange coupling

$$\rho_0 J = \frac{4\Gamma}{\pi} e^{-(\lambda/\omega_0)^2} \sum_{\bar{n}_b=0}^{\infty} \frac{1}{\bar{n}_b!} \frac{(\lambda/\omega_0)^{2\bar{n}_b}}{\bar{U}/2 + \bar{n}_b\,\omega_0}, \tag{31}$$

representing a sum over virtual transitions of the impurity from occupation $n_d = 1$ to $n_d = 0$ or 2, accompanied by excitation of different numbers $\bar{n}_b = 0, 1, \ldots$ of bosonic quanta. To facilitate comparison with the corresponding expression $\rho_0 J = 8\Gamma/\pi U$ for the symmetric Anderson model without bosons, one can use Eq. (20) to recast Eq. (31) in the form

$$\rho_0 J = \frac{8\Gamma}{\pi|\bar{U}|} S\left(\frac{|\bar{U}|}{2\omega_0}, \frac{\varepsilon_p}{\omega_0}\right) \equiv \frac{8\Gamma}{\pi U_{\rm eff}}, \tag{32}$$

where, both for $\bar{U} > 0$ (as is the case here) and for $\bar{U} < 0$,

$$U_{\rm eff} = 2\,\mathcal{E}(|\bar{U}|/2) \tag{33}$$

with $\mathcal{E}(E)$ as defined in Eq. (19). Equation (32) suggests that $U_{\rm eff}$ plays the role of an effective Coulomb repulsion in the

low-energy many-body physics of the full Anderson-Holstein model, distinct from the quantity $\bar{U}$ [Eq. (9)] that emerges from considering just the atomic limit $\Gamma = 0$. Like $\bar{U}$, $U_{\rm eff}$ passes through zero at $\lambda = \lambda_0$. For fixed U, the ratio $U_{\rm eff}/\bar{U}$ evolves smoothly from 1 for $\lambda = 0$ to $e^{U/2\omega_0}$ ($\simeq$12 in the case $U/2\omega_0 = 2.5$ used in our calculations) for $\lambda = \lambda_0$ to 2 for $\lambda \to \infty$.

Extension of the analysis of Ref. 50 to the case of a pseudogap density of states leads to the conclusion that the critical hybridization width separating the local-moment and symmetric strong-coupling phases should satisfy

$$\Gamma_c = \frac{\pi}{4} j_c(r)\, D \left(\frac{U_{\rm eff}}{2D}\right)^{1-r}. \tag{34}$$

The solid lines plotted in Fig. 4 show the boundaries predicted by Eq. (34) with numerical evaluation of $U_{\rm eff}$. The agreement with the NRG data points is excellent for all four values of r, and for λ extending from zero almost all the way to λ_0.

2. Strong bosonic coupling

Cornaglia *et al.* have demonstrated[50] that the Anderson-Holstein model with $\lambda \gg \lambda_0$ maps to a charge analog of the Kondo model in which the impurity isospin degree of freedom [the impurity (d-electron) parts of the operators defined in Eqs. (28)] is screened by its conduction-band counterpart. The impurity-band isospin exchange is anisotropic, with a longitudinal coupling $\rho_0 J_z = 8\Gamma/\pi|U_{\rm eff}|$ and a transverse coupling

$$\rho_0 J_\perp = \frac{8\Gamma}{\pi|\bar{U}|}\, S\left(\frac{|\bar{U}|}{2\omega_0}, -\frac{\varepsilon_p}{\omega_0}\right) \sim e^{-2\varepsilon_p/\omega_0}\, \rho_0 J_z, \tag{35}$$

where $U_{\rm eff}$ and $S(a,x)$ are defined in Eqs. (33) and (20), respectively. Closer investigation shows that an approximation that is equivalent for large λ but also remains valid much closer to λ_0 is

$$J_\perp \simeq e^{-|U_{\rm eff}|/2\omega_0} J_z. \tag{36}$$

The strong suppression of "charge-flip" scattering arises from the exponentially small overlap between the ground state of the displaced harmonic oscillator that minimizes the electron-boson interaction in the sector $n_d = 0$ and the corresponding ground state for $n_d = 2$ (see Sec. II B 2).

A poor-man's scaling analysis of the anisotropic pseudogap Kondo model[62] indicates that for $J_z \gg |J_\perp|$, the phase boundary is defined by a condition $\rho_0 J_z \simeq r \ln(2J_z/J_\perp)$. Applying this condition to the pseudogap Anderson-Holstein model, carrying over Eq. (36) from the case $r = 0$, and assuming [by analogy with Eq. (29)] that $\rho_0 J_z \propto |U_{\rm eff}/D|^{r-1}$, yields

$$\Gamma_{c2}(\lambda) \sim \left|\frac{U_{\rm eff}}{D}\right|^{2-r} \sim \lambda^{2(2-r)}, \tag{37}$$

where we have used $U_{\rm eff} \simeq 2\bar{U} \simeq -4\,\varepsilon_p = -4\lambda^2/\omega_0$ for $\lambda \gg \lambda_0$. The validity of Eq. (37) is questionable because the critical hybridization widths it demands are too large to justify mapping to a Kondo model. Nonetheless, the NRG data for each value of r plotted in Fig. 4 follow a $\lambda^{2(2-r)}$ dependence (dashed lines) quite closely for $0.2 \leqslant \lambda \leqslant 0.4$. (This power law must break down closer to the level crossing between the local-moment and local-charge phases because Γ_{c2} necessarily vanishes at $\lambda = \lambda_0$.)

C. Crossover scales

Aside from allowing the identification of renormalization-group fixed points and phase boundaries, the eigenspectrum of $\hat{H}_N$ can also be used to define temperature scales characterizing crossovers between the domains of influence of different fixed points. We focus on the smallest such scale, which describes the approach to one of the stable fixed points of the problem.

1. Weak bosonic coupling

With decreasing $|\Gamma - \Gamma_{c1}|$, E_N in Fig. 2(a) remains close to its critical value E_c over an increasing number of iterations before heading either to $E_{\rm LM}$ or to $E_{\rm SSC}$. To quantify this effect, it is useful to define threshold energy values $E_\pm$ where $E_{\rm LM} < E_- < E_c < E_+ < E_{\rm SSC}$. The passage of E_N below E_- (above E_+) at some N_1^*, determined by interpolation of the NRG data at even integer values of N, can be taken to mark the crossover around temperature $T_1^* \simeq D\Lambda^{-N_1^*/2}$ from an intermediate-temperature quantum-critical regime dominated by the unstable critical point C_S to a low-temperature regime controlled by the stable local-moment (symmetric strong-coupling) fixed point. This crossover scale is expected to vanish for $\Gamma \to \Gamma_{c1}$, as shown schematically in Fig. 2(b). Figure 2(c) plots values of T_1^* determined by the criterion $E_- = 0.3$, $E_+ = 0.8$. These data are consistent with the relation

$$T_1^* \propto |\Gamma - \Gamma_{c1}|^{\nu_1} \quad \text{as} \quad \Gamma \to \Gamma_{c1}, \tag{38}$$

where ν_1 is the correlation-length exponent at the quantum-critical point. The numerical value of ν_1 is independent of the precise choice of the thresholds $E_\pm$. What is more, different combinations of the model parameters r, U, ω_0, and λ result in different critical couplings Γ_{c1}, but ν_1 depends only on the band exponent r. Values for three representative cases are listed in Table I.

2. Strong bosonic coupling

The passage of E_N outside a range $E_- < E_N < E_+$ can also be used to define a crossover scale near its charge-sector critical point. This scale T_2^* is expected to vanish at the critical point according to

$$T_2^* \propto |\Gamma - \Gamma_{c2}|^{\nu_2} \quad \text{as} \quad \Gamma \to \Gamma_{c2}, \tag{39}$$

a behavior that is sketched qualitatively in Fig. 3(b) and is confirmed quantitatively in Fig. 3(c). For all the values of r

TABLE I. Critical exponents at the critical point C_S of the particle-hole-symmetric pseudogap Anderson-Holstein model, evaluated for three band exponents r. The critical exponents are defined in Eqs. (38) and (42). A number in parentheses indicates the estimated random error in the last digit of each exponent.

r	ν_1	β_1	$1/\delta_1$	x_1	γ_1
0.2	6.22(1)	0.15(1)	0.02630(2)	0.9488(2)	5.85(6)
0.3	5.14(1)	0.34(1)	0.07364(1)	0.8629(3)	4.41(3)
0.4	5.84(1)	0.90(1)	0.1845(1)	0.6885(2)	3.95(5)

and Λ that we have studied, the numerical values of ν_1 and ν_2 coincide to within our estimated errors.

D. Impurity thermodynamic properties

This section addresses the variation with temperature of the impurity contributions[56] to the static spin and charge susceptibilities and to the entropy. With the conventional definitions $T\chi_{s,\mathrm{imp}} = \langle \hat{S}_z^2 \rangle$ and $T\chi_{c,\mathrm{imp}} = \langle Q^2 \rangle$, a symmetric impurity level isolated from the conduction band ($\Gamma = 0$) has $T\chi_{s,\mathrm{imp}} = \frac{1}{4}$ and $T\chi_{c,\mathrm{imp}} = 0$ for $U_{\mathrm{eff}} \gg T$, but $T\chi_{c,\mathrm{imp}} = 1$ and $T\chi_{s,\mathrm{imp}} = 0$ for $U_{\mathrm{eff}} \ll -T$, with U_{eff} as defined in Eq. (33). Due to the factor of 4 difference between the local-moment spin susceptibility and the charge susceptibility of a local charge doublet, it is most appropriate to compare $T\chi_{s,\mathrm{imp}}$ with $\frac{1}{4}T\chi_{c,\mathrm{imp}}$. During the NRG calculation of these thermodynamic properties, $N_s = 3000$ states were retained after each iteration.

1. Weak bosonic coupling

Figure 5 plots the temperature dependence of $T\chi_{s,\mathrm{imp}}$, $\frac{1}{4}T\chi_{c,\mathrm{imp}}$, and S_{imp} for $r = 0.4$, $\lambda = 0.05$, and seven values of Γ straddling Γ_{c1}. At high temperatures $T \gg \max(U_{\mathrm{eff}}, \Gamma)$, the properties lie close to those of the free-orbital fixed point ($T\chi_{s,\mathrm{imp}} = \frac{1}{4}T\chi_{c,\mathrm{imp}} = \frac{1}{8}$ and $S_{\mathrm{imp}} = \ln 4$), irrespective of the specific value of Γ. However, the $T \to 0$ behaviors directly reflect the existence of a QPT at $\Gamma = \Gamma_{c1}$. In the local-moment phase ($\Gamma < \Gamma_{c1}$), the residual impurity spin doublet is revealed in the limiting behaviors $T\chi_{s,\mathrm{imp}} = \frac{1}{4}$, $\frac{1}{4}T\chi_{c,\mathrm{imp}} = 0$, and $S_{\mathrm{imp}} = \ln 2$. In the symmetric strong-coupling phase ($\Gamma > \Gamma_{c1}$), the impurity degrees of freedom are quenched to the maximum extent possible given the power-law hybridization function,[14] yielding $T\chi_{s,\mathrm{imp}} = \frac{1}{4}T\chi_{c,\mathrm{imp}} = r/8$ and $S_{\mathrm{imp}} = 2r \ln 2$. Exactly at $\Gamma = \Gamma_{c1}$, the low-temperature properties are distinct from those in either phase: $T\chi_{s,\mathrm{imp}} \simeq 0.1348$, $\frac{1}{4}T\chi_{c,\mathrm{imp}} \simeq 0.0158$, and $S_{\mathrm{imp}} \simeq 0.694 \simeq \ln 2$. These values vary with the band exponent r, but are independent of other model parameters such as U, ω_0, and λ, so they can be regarded as characterizing the critical point $\mathrm{C_S}$. For all the r values that we have examined, the critical properties coincide with those at the corresponding critical point of the pseudogap Kondo or Anderson models.[14]

When Γ deviates slightly from Γ_{c1}, the thermodynamic properties follow their critical behaviors at high temperatures, but cross over for $T \lesssim T_1^*$ to approach the values characterizing the local-moment or symmetric strong-coupling phase. The crossover temperature T_1^* coincides up to a constant multiplicative factor with that extracted from the NRG spectrum (as described in Sec. III B) and its variation with $|\Gamma - \Gamma_{c1}|$ yields, via Eq. (38), a correlation-length exponent $\nu_1(r)$ in agreement with the values listed in Table I.

2. Strong bosonic coupling

Figure 6 plots the temperature dependence of $T\chi_{s,\mathrm{imp}}$, $\frac{1}{4}T\chi_{c,\mathrm{imp}}$, and S_{imp} for $r = 0.4$, $\lambda = 0.2$, and various Γ straddling the critical value Γ_{c2}. Like in the case of weak bosonic coupling, the $T \to 0$ behaviors distinguish the two stable phases: the properties $T\chi_{s,\mathrm{imp}} = 0$, $\frac{1}{4}T\chi_{c,\mathrm{imp}} = \frac{1}{4}$, and $S_{\mathrm{imp}} = \ln 2$ in the local-charge phase contrast with $T\chi_{s,\mathrm{imp}} = \frac{1}{4}T\chi_{c,\mathrm{imp}} = r/8$ and $S_{\mathrm{imp}} = 2r \ln 2$ in the symmetric strong-coupling phase. Exactly at $\Gamma = \Gamma_{c2}$, $T\chi_{s,\mathrm{imp}} \simeq$

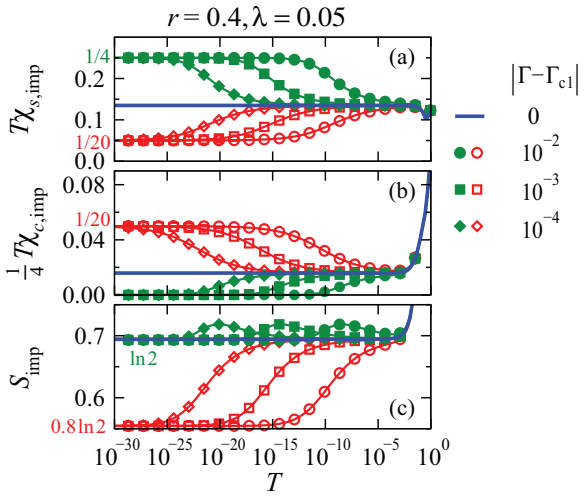

FIG. 5. (Color online) Thermodynamic properties of the particle-hole-symmetric pseudogap Anderson-Holstein model near its spin-sector critical point $\mathrm{C_S}$: Temperature dependence of the impurity contribution to (a) the static spin susceptibility $\chi_{s,\mathrm{imp}}$ multiplied by temperature, (b) the static charge susceptibility $\chi_{c,\mathrm{imp}}$ multiplied by temperature, and (c) the entropy S_{imp}, for $r = 0.4$, $U = -2\varepsilon_d = 0.5$, $\omega_0 = 0.1$, $\lambda = 0.05 < \lambda_0 \simeq 0.158$, and the seven values of $\Gamma - \Gamma_{c1}$ labeled in the legend. Filled (open) symbols connected by guiding lines represent data in the local-moment (symmetric strong-coupling) phase, while thick lines without symbols show the critical properties at $\mathrm{C_S}$. $N_s = 3000$ states were retained after each NRG iteration.

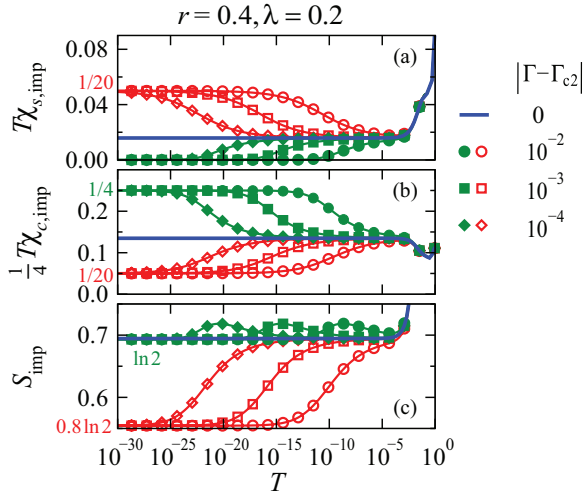

FIG. 6. (Color online) Thermodynamic properties of the particle-hole-symmetric pseudogap Anderson-Holstein model near its charge-sector critical point $\mathrm{C_C}$: Temperature dependence of the impurity contribution to (a) the static spin susceptibility $\chi_{s,\mathrm{imp}}$ multiplied by temperature, (b) the static charge susceptibility $T\chi_{c,\mathrm{imp}}$ multiplied by temperature, and (c) the entropy S_{imp}, for $r = 0.4$, $U = -2\varepsilon_d = 0.5$, $\omega_0 = 0.1$, $\lambda = 0.2 > \lambda_0 \simeq 0.158$, and the seven values of $\Gamma - \Gamma_{c2}$ labeled in the legend. Filled (open) symbols connected by guiding lines represent data in the local-charge (symmetric strong-coupling) phase, while thick lines without symbols show the critical properties at $\mathrm{C_C}$. $N_s = 3000$ states were retained after each NRG iteration.

0.0158, $\frac{1}{4}T\chi_{c,\mathrm{imp}} \simeq 0.1348$, and $S_{\mathrm{imp}} \simeq 0.694$, values that can be taken to characterize the critical point $\mathrm{C_C}$. From the thermodynamics near $\mathrm{C_C}$, one can extract a crossover scale T_2^* that gives [via Eq. (39)] a correlation-length exponent ν_2 identical to that determined from the NRG spectrum.

Figures 5 and 6 illustrate the general property that the temperature dependence of the spin (charge) susceptibility at $\mathrm{C_S}$ mirrors that of the charge (spin) susceptibility at $\mathrm{C_C}$, while the entropy behaves in the same manner at both critical points. These observations are consistent with the equivalence of the NRG spectra at the two fixed points under interchange of spin and charge quantum numbers (see Sec. III A).

E. Local response and universality class

In order to investigate in greater detail the properties of the spin and charge critical points ($\mathrm{C_S}$ and $\mathrm{C_C}$ in Fig. 10), it is necessary to identify an appropriate order parameter for each QPT. The symmetric strong-coupling and local-moment phases can be distinguished by their values (0 and $\frac{1}{2}$, respectively) of the magnitude $|\langle S_z\rangle|$ of the total spin in a vanishingly small magnetic field applied along the z direction. Similarly, the magnitude $|\langle Q\rangle|$ of the total charge in the presence of an infinitesimal electric potential takes the value 0 in the symmetric strong-coupling phase and 1 in the local-charge phase. However, the fact that S_z and Q are conserved quantities, i.e., that the pseudogap Anderson-Holstein Hamiltonian commutes with $\hat{S}_z$ and $\hat{Q}$ defined in Eqs. (25) and (26), respectively, prevents these candidate order parameters from exhibiting nontrivial critical exponents.[68,69] Instead, we must look to the impurity response to local fields in order to probe the quantum-critical behavior.

1. Weak bosonic coupling

In the pseudogap Kondo and Anderson models, the critical properties manifest themselves[23] through the response to a local magnetic field h that couples only to the impurity spin as specified in Eq. (6). The order parameter for the pseudogap QPT is the limiting value as $h \to 0$ of the local moment

$$M_{\mathrm{loc}} = \left\langle \tfrac{1}{2}(\hat{n}_{d\uparrow} - \hat{n}_{d\downarrow}) \right\rangle, \tag{40}$$

and the order-parameter susceptibility is the static local-spin susceptibility

$$\chi_{s,\mathrm{loc}} = -\lim_{h\to 0} \frac{M_{\mathrm{loc}}}{h}. \tag{41}$$

Based on the similarities noted above between the pseudogap Anderson critical point and the $\mathrm{C_S}$ critical point of the pseudogap Anderson-Holstein model (i.e., the properties of the phases on either side of each transition, the NRG spectrum at the transition, and the value of the order-parameter exponent), we expect that the two QPTs also share the same order parameter. Accordingly, the behaviors of M_{loc} and $\chi_{s,\mathrm{loc}}$ in the vicinity of the critical hybridization width $\Gamma = \Gamma_{c1}$ should be described by critical exponents β_1, γ_1, δ_1, and x_1 defined as follows:

$$M_{\mathrm{loc}}(\Gamma < \Gamma_{c1}; h \to 0, T = 0) \propto (\Gamma_{c1} - \Gamma)^{\beta_1}, \tag{42a}$$

$$\chi_{s,\mathrm{loc}}(\Gamma > \Gamma_{c1}; T = 0) \propto (\Gamma - \Gamma_{c1})^{-\gamma_1}, \tag{42b}$$

$$M_{\mathrm{loc}}(h; \Gamma = \Gamma_{c1}, T = 0) \propto |h|^{1/\delta_1}, \tag{42c}$$

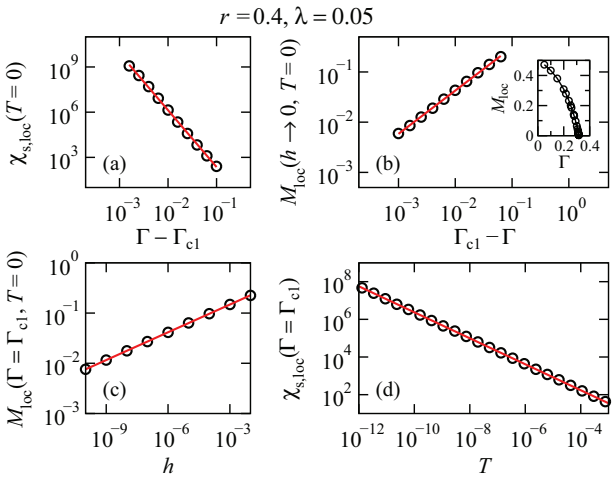

FIG. 7. (Color online) Static local-spin response of the particle-hole-symmetric pseudogap Anderson-Holstein model near its spin-sector critical point $\mathrm{C_S}$. Circles are NRG data for $r = 0.4$, $U = -2\varepsilon_d = 0.5$, $\omega_0 = 0.1$, and $\lambda = 0.05$, at or near the critical hybridization width $\Gamma_{c1} \simeq 0.316\,680\,5$. Straight lines represent power-law fits. (a) Static local-spin susceptibility $\chi_{s,\mathrm{loc}}(T = 0)$ vs $\Gamma - \Gamma_{c1}$ in the symmetric strong-coupling phase. (b) Local magnetization $M_{\mathrm{loc}}(h \to 0, T = 0)$ vs $\Gamma_{c1} - \Gamma$ in the local-moment phase. Inset: Continuous vanishing of $M_{\mathrm{loc}}(h \to 0, T = 0)$ as Γ approaches Γ_{c1} from below. (c) Local magnetization $M_{\mathrm{loc}}(\Gamma = \Gamma_{c1}, T = 0)$ vs local magnetic field h. (d) Static local-spin susceptibility $\chi_{s,\mathrm{loc}}(\Gamma = \Gamma_c)$ vs temperature T.

$$\chi_{s,\mathrm{loc}}(T; \Gamma = \Gamma_{c1}) \propto T^{-x_1}. \tag{42d}$$

The preceding expectations are proved correct by NRG calculations, as demonstrated in Fig. 7 for $r = 0.4$ and $\lambda = 0.05$, the case treated in Fig. 2. The critical exponents extracted as best-fit slopes of log-log plots are listed in Table I for three values of the band exponent r. The values of individual critical exponents vary with r, but are independent of other Hamiltonian parameters (U, ω_0, and λ) and are well converged with respect to the NRG parameters (Λ, N_s, and N_b). To within their estimated accuracy, the critical exponents for a given r obey the hyperscaling relations

$$\delta_1 = \frac{1 + x_1}{1 - x_1}, \quad 2\beta_1 = \nu(1 - x_1), \quad \gamma_1 = \nu_1 x_1, \tag{43}$$

which are consistent with the scaling ansatz

$$F = T\,\mathcal{F}\left(\frac{|\Gamma - \Gamma_{c1}|}{T^{1/\nu_1}}, \frac{|h|}{T^{(1+x_1)/2}}\right) \tag{44}$$

for the nonanalytic part of the free energy at an interacting critical point.[23]

2. Strong bosonic coupling

We have seen above that the NRG spectrum and low-temperature thermodynamics at the $\mathrm{C_C}$ fixed point are related to those at the $\mathrm{C_S}$ fixed point by interchange of spin and charge degrees of freedom. One therefore expects to be able to probe the critical properties via the response to a local electric potential ϕ that enters the model through an additional

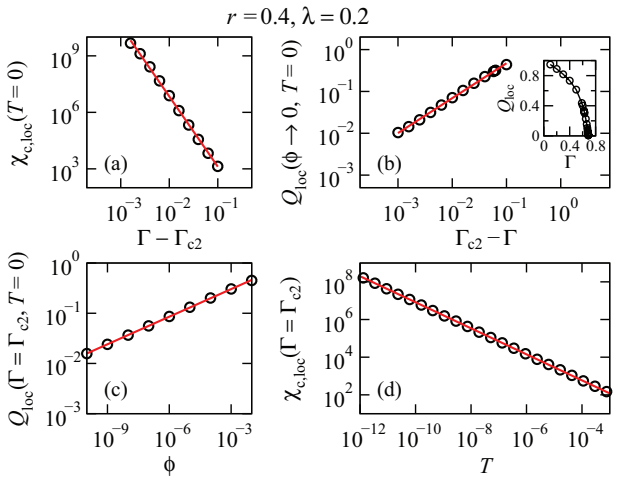

FIG. 8. (Color online) Static local charge response of the particle-hole-symmetric pseudogap Anderson-Holstein model near its charge-sector critical point C_C. Circles are NRG data for $r = 0.4$, $U = -2\varepsilon_d = 0.5$, $\omega_0 = 0.1$, and $\lambda = 0.2$, at or near the critical hybridization width $\Gamma_{c2} \simeq 0.687\,895\,6$. Straight lines represent power-law fits. (a) Static local charge susceptibility $\chi_{c,\mathrm{loc}}(T = 0)$ vs $\Gamma - \Gamma_{c2}$ in the symmetric strong-coupling phase. (b) Local charge $Q_{\mathrm{loc}}(\phi \to 0, T = 0)$ vs $\Gamma_{c2} - \Gamma$ in the local-charge phase. Inset: Continuous vanishing of $Q_{\mathrm{loc}}(\phi \to 0, T = 0)$ as Γ approaches Γ_{c2} from below. (c) Local charge $Q_{\mathrm{loc}}(\Gamma = \Gamma_{c2}, T = 0)$ vs local electric potential ϕ. (d) Static local charge susceptibility $\chi_{c,\mathrm{loc}}(\Gamma = \Gamma_{c2})$ vs temperature T.

Hamiltonian term

$$\hat{H}_\phi = \phi(\hat{n}_d - 1). \tag{45}$$

Comparison with Eq. (2a) shows that ϕ is equivalent to a shift in δ_d (or ε_d). The order parameter should be the $\phi \to 0$ limiting value of the local charge

$$Q_{\mathrm{loc}} = \langle \hat{n}_d - 1 \rangle, \tag{46}$$

and the order-parameter susceptibility should be the static local charge susceptibility

$$\chi_{c,\mathrm{loc}} = -\lim_{\phi \to 0} \frac{Q_{\mathrm{loc}}}{\phi}. \tag{47}$$

In the vicinity of the critical point $\Gamma = \Gamma_{c2}$, one expects the following critical behaviors:

$$Q_{\mathrm{loc}}(\Gamma < \Gamma_{c2}; \phi \to 0, T = 0) \propto (\Gamma_{c2} - \Gamma)^{\beta_2}, \tag{48a}$$

$$\chi_{c,\mathrm{loc}}(\Gamma > \Gamma_{c2}; T = 0) \propto (\Gamma - \Gamma_{c2})^{-\gamma_2}, \tag{48b}$$

$$Q_{\mathrm{loc}}(\phi; \Gamma = \Gamma_{c2}, T = 0) \propto |\phi|^{1/\delta_2}, \tag{48c}$$

$$\chi_{c,\mathrm{loc}}(T; \Gamma = \Gamma_{c2}) \propto T^{-x_2}. \tag{48d}$$

These expectations are borne out by the NRG results, as illustrated in Fig. 8 for the case $r = 0.4$, $\lambda = 0.2$ treated in Fig. 3.

3. *Comparison between weak and strong bosonic coupling*

Figure 9(a) superimposes the variation with Γ of the order parameter in the vicinity of the C_S and C_C critical points for two representative band exponents $r = 0.2$ and 0.4. The equality of the slopes of the log-log plots at the spin- and charge-sector QPTs shows that $\beta_1 = \beta_2$. Similarly, Fig. 9(b) shows that the temperature variation of the order-parameter susceptibilities

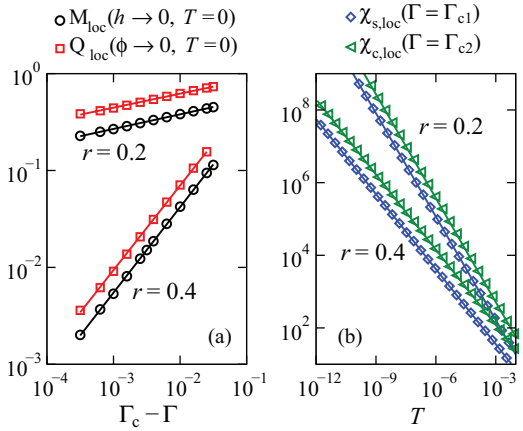

FIG. 9. (Color online) Comparison of the static local responses of the particle-hole-symmetric pseudogap Anderson-Holstein model near its critical points C_S and C_C: (a) Dependence of the local magnetization $M_{\mathrm{loc}}(h \to 0, T = 0)$ on $\Gamma_{c1} - \Gamma$ and of the local charge $Q_{\mathrm{loc}}(\phi \to 0, T = 0)$ on $\Gamma_{c2} - \Gamma$, for $U = -2\varepsilon_d = 0.5$, $\omega_0 = 0.1$, $\lambda = 0.05$ (magnetic response) or 0.2 (charge response), and band exponents $r = 0.2$ and 0.4. (b) Static local-spin susceptibility $\chi_{s,\mathrm{loc}}(T; \Gamma = \Gamma_{c1})$ and static local charge susceptibility $\chi_{c,\mathrm{loc}}(T; \Gamma = \Gamma_{c2})$ vs temperature T. All parameters other than Γ take the same values as in (a). Straight lines represent power-law fits.

is consistent with $x_1 = x_2$. Indeed, for each value of r that we have examined, we find that all critical exponents at C_C are indistinguishable (within our estimated errors) from the corresponding exponents at C_S and at the critical point of the pseudogap Kondo model (as given in Table I of Ref. 23). This leads us to conclude that all three critical points lie in the same universality class.

F. Renormalization-group flows

The essential physics of the particle-hole-symmetric pseudogap Anderson-Holstein model can be summarized in the schematic renormalization-group flow diagram shown in Fig. 10, which applies to all band exponents in the range $0 < r < \frac{1}{2}$. Arrows indicate the evolution of the effective Coulomb interaction U_{eff} and the hybridization width Γ with increasing NRG iteration number N, i.e., under progressive reduction of the temperature $T \simeq D\Lambda^{-N/2}$. The high-temperature limit of the model is governed by the *free-orbital* (FO) fixed point, corresponding to bare model parameters $U = \Gamma = \lambda = 0$ and a Fermi-level phase shift $\delta_0(0) = 0$. Dashed lines mark the separatrices between the basins of attraction of the local-moment (LM), local-charge (LC), and symmetric strong-coupling (SSC) fixed points described above. Flow along each separatrix is from the free-orbital fixed point towards one or other of two quantum-critical points: either the conventional spin-sector critical point C_S reached for $U_{\mathrm{eff}} > 0$ or its charge analog C_C reached for $U_{\mathrm{eff}} < 0$.

A renormalization-group fixed-point structure equivalent to that described in the preceding paragraph has been presented previously[25] for the pseudogap Anderson model under the assumption that the bare onsite Coulomb interaction U may be taken to be positive or negative. Indeed, many of the universal properties of the pseudogap Anderson-Holstein

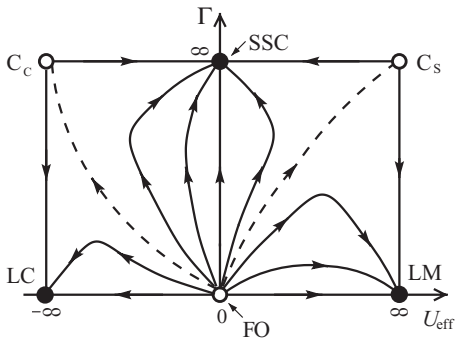

FIG. 10. Schematic renormalization-group flows on the $U_{\rm eff}$-Γ plane for the particle-hole-symmetric pseudogap Anderson-Holstein model with a band exponent $0 < r < \frac{1}{2}$. Trajectories with arrows represent the flow of the couplings with decreasing temperature. Dashed lines connecting unstable fixed points (open circles) separate the basins of attraction of stable fixed points (filled circles). The right and left dashed lines represent the boundary values Γ_{c1} and Γ_{c2} defined in Eqs. (34) and (37), respectively. The asymmetry of the flows about the line $U_{\rm eff} = 0$ stems from differing symmetries of the model in the spin and charge sectors. See the text for a discussion of each fixed point.

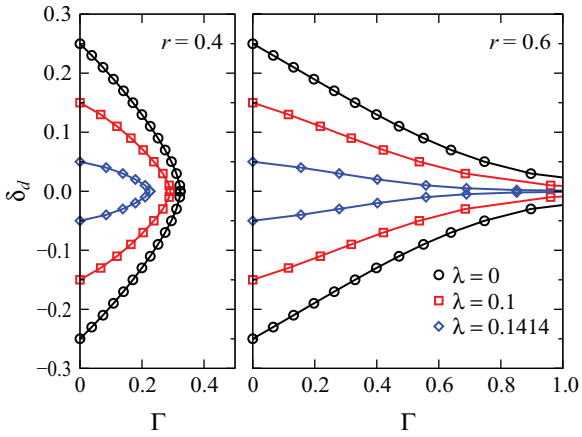

FIG. 11. (Color online) Phase boundaries of the zero-field pseudogap Anderson-Holstein model on the Γ-δ_d plane for weak bosonic couplings $\lambda < \lambda_0 = 0.15812(1)$ and band exponent $r = 0.4$ (left), $r = 0.6$ (right). Data calculated for $U = 0.5$, $h = 0$, $\omega_0 = 0.1$, and the three values of λ listed in the legend.

model presented in this section, particularly ones associated with the quantum-critical points C_S and C_C, reproduce those of this extended pseudogap Anderson model.

However, we emphasize that the particle-hole-symmetric Anderson and Anderson-Holstein models have different symmetries and are therefore not trivially related to one another. The pseudogap Anderson Hamiltonian exhibits exact SU(2) spin and isospin (charge) symmetries, and all physical properties at a point (U,Γ) in the diagram analogous to Fig. 10 [see Fig. 1(b) of Ref. 25] map exactly to the properties at $(-U,\Gamma)$ under the interchange of spin and charge degrees of freedom. No such mapping holds in the pseudogap Anderson-Holstein model, where the Hamiltonian has full SU(2) spin symmetry but only a discrete charge symmetry. This distinction leads, for instance, to the critical hybridization width Γ_{c1} having a sublinear dependence on $U_{\rm eff}$ [Eq. (34)], whereas its counterpart Γ_{c2} is superlinear in $U_{\rm eff}$ [Eq. (37)]. The equivalence of the critical points C_S and C_C under spin-charge interchange signals the emergence of a higher SU(2) isospin symmetry at both these renormalization-group fixed points.

For $r \geqslant \frac{1}{2}$, we find that (just as in the pseudogap Anderson model[25]) the symmetric strong-coupling fixed point of the pseudogap Anderson-Holstein model is unstable with respect to any breaking of degeneracy between the four impurity levels, i.e., to any $U_{\rm eff} \neq 0$. As a result, the $U_{\rm eff}$-Γ plane is divided into just two phases: local moment for all $U_{\rm eff} > 0$ and local charge for all $U_{\rm eff} < 0$.

IV. RESULTS: GENERAL MODEL WITH BAND EXPONENT $0 < r < 1$

This section treats the pseudogap Anderson-Holstein model with a band exponent $0 < r < 1$ when either (the discrete) particle-hole symmetry is broken by a value $\delta_d \equiv \varepsilon_d + \frac{1}{2}U \neq 0$ or (the continuous) spin-rotation invariance is removed by a nonvanishing local magnetic field h [defined in Eq. (6)]. It is found that increasing $|\delta_d|$ or $|h|$ can drive the system from the local-moment or local-charge phase into one of several strong-coupling phases that are not present in the baseline case $\delta_d = h = 0$. The transitions between these phases take place at interacting quantum-critical points in the same universality class as the asymmetric critical points of the pseudogap Anderson model.

All numerical results presented in this section were obtained for an impurity with $U = 0.5$, for a bosonic energy $\omega_0 = 0.1$, and for NRG discretization parameter $\Lambda = 3$.

A. Phase boundaries

1. Weak bosonic coupling

Figure 11 plots phase boundaries of the pseudogap Anderson-Holstein model on the Γ-δ_d plane for zero magnetic field, for band exponents $r = 0.4$ (left) and 0.6 (right), and for three bosonic couplings $\lambda = 0$, 0.1, and 0.1414 that can all be associated [via Eq. (9)] with effective Coulomb interactions $\bar{U} > 0$. A value $\delta_d \neq 0$ breaks particle-hole symmetry but leaves in place the SU(2) spin symmetry. The system remains in the local-moment phase for $|\delta_d| < \frac{1}{2}\bar{U}$ and $\Gamma < \Gamma_{c1}(r,U,\delta_d,\lambda) \equiv \Gamma_{c1}(r,U,-\delta_d,\lambda)$. Otherwise, it lies in one of the strong-coupling phases described in Sec. II B 1: symmetric strong-coupling for $\delta_d = 0$, ASC$_-$ for $\delta_d > 0$, or ASC$_+$ for $\delta_d < 0$. Just as in the pseudogap Anderson model,[14] the symmetric strong-coupling phase can be reached only for $r < \frac{1}{2}$; for $r \geqslant \frac{1}{2}$, the symmetric strong-coupling fixed point is unstable and $\Gamma_{c1}(r,U,\delta_d)$ diverges as δ_d approaches zero. The contraction of the local-moment phase (i.e., the reduction of Γ_{c1}) with increasing λ and/or $|\delta_d|$ can be attributed to one or both of the $n_d \neq 1$ impurity levels being drawn down in energy closer to the $n_d = 1$ ground states. This energy shift enhances indirect spin-flip scattering between the ground states via the excited states and favors conduction-band quenching of the impurity degrees of freedom.

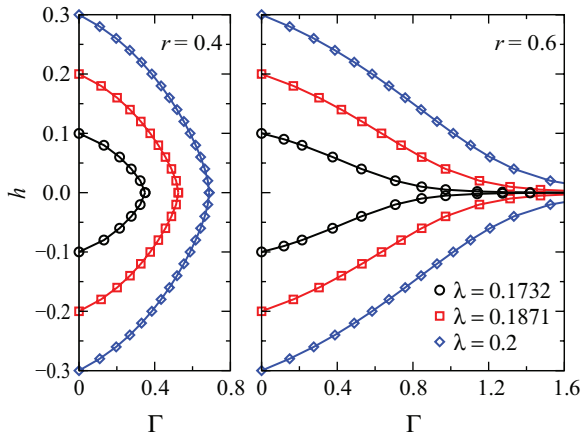

FIG. 12. (Color online) Phase boundaries of the particle-hole-symmetric pseudogap Anderson-Holstein model on the Γ-h plane for strong bosonic couplings $\lambda > \lambda_0 = 0.15812(1)$ and band exponent $r = 0.4$ (left), $r = 0.6$ (right). Data calculated for $U = -2\epsilon_d = 0.5$, $\omega_0 = 0.1$, and the three values of λ listed in the legend.

2. Strong bosonic coupling

Figure 12 plots phase boundaries of the particle-hole-symmetric pseudogap Anderson-Holstein model on the Γ-h plane for $r = 0.4$ (left) and 0.6 (right), and for three strong bosonic couplings in the range $\lambda > \lambda_0$. Here, Eq. (9) gives $\bar{U} < 0$, and for local magnetic field $h = 0$, the lowest-energy impurity states are spinless but have a charge $Q = \pm 1$. Application of a field $h \neq 0$ destroys SU(2) spin symmetry but preserves particle-hole symmetry. The field pulls one or other of the $Q = 0$ excited states down in energy, thereby enhancing virtual scattering between the $Q = \pm 1$ states. The model remains in the local-charge phase for $|h| < |\bar{U}|$ and $\Gamma < \Gamma_{c2}(r,U,h,\lambda) \equiv \Gamma_{c2}(r,U,-h,\lambda)$. Otherwise, it lies in the symmetric strong-coupling phase (for $r < \frac{1}{2}$ and $h = 0$) or in one of two new asymmetric strong-coupling phases: $\mathrm{ASC}_\downarrow$ with ground-state spin z component $S_z = -\frac{1}{2}$ for $h > 0$, or $\mathrm{ASC}_\uparrow$ with $S_z = \frac{1}{2}$ for $h < 0$. For $r \geqslant \frac{1}{2}$, $\Gamma_{c2}(r,U,h,\lambda)$ diverges as h approaches zero, a consequence of the instability of the symmetric strong-coupling fixed point in this range of band exponents.

Although the two panels of Fig. 12 look quite similar to their counterparts in Fig. 11, there are small departures such as the absence from Γ_{c1} versus δ_d for $r = 0.6$ of points of inflection corresponding to those seen in Γ_{2c} versus h. These differences presumably arise from the differing symmetries of the two cases.

B. Impurity thermodynamic properties

1. Weak bosonic coupling

Figure 13 plots the temperature dependence of $T\chi_{s,\mathrm{imp}}$, $\frac{1}{4}T\chi_{c,\mathrm{imp}}$, and S_{imp} for $r = 0.4$, $U = 0.5$, $\varepsilon_d = -0.2$ (or $\delta_d = 0.05 > 0$), $\lambda = 0.05$, and seven values of Γ straddling Γ_{c1}. The low-temperature limiting behaviors in the local-moment phase ($\Gamma < \Gamma_{c1}$) are identical to those found at particle-hole symmetry (see Fig. 5). In the ASC_- phase ($\Gamma > \Gamma_{c1}$), however, the $T = 0$ properties $T\chi_{s,\mathrm{imp}} = \frac{1}{4}T\chi_{c,\mathrm{imp}} = S_{\mathrm{imp}} = 0$ indicate complete quenching of the impurity degrees of

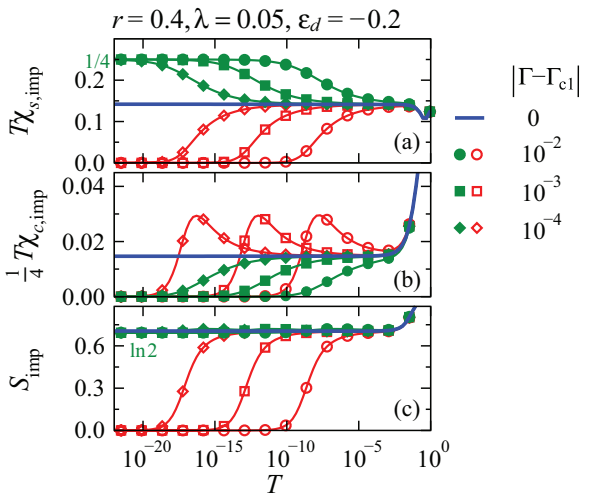

FIG. 13. (Color online) Thermodynamic properties of the particle-hole-asymmetric pseudogap Anderson-Holstein model in zero magnetic field near the spin-sector critical point C_-: Temperature dependence of the impurity contribution to (a) the static spin susceptibility $\chi_{s,\mathrm{imp}}$ multiplied by temperature, (b) the static charge susceptibility $\chi_{c,\mathrm{imp}}$ multiplied by temperature, and (c) the entropy S_{imp}, for $r = 0.4$, $\varepsilon_d = -0.2$, $U = 0.5$, $\omega_0 = 0.1$, $\lambda = 0.05 < \lambda_0 \simeq 0.158$, and the seven values of $\Gamma - \Gamma_{c1}$ labeled in the legend. Filled (open) symbols connected by guiding lines represent data in the local-moment (ASC_-) phase, while thick lines without symbols show the critical properties at C_-. $N_s = 3000$ states were retained after each NRG iteration.

freedom, in contrast to the partial quenching found in the symmetric strong-coupling phase. Exactly at $\Gamma = \Gamma_{c1}$, the low-temperature properties $T\chi_{s,\mathrm{imp}} \simeq 0.1419$, $\frac{1}{4}T\chi_{c,\mathrm{imp}} \simeq 0.0147$, and $S_{\mathrm{imp}} \simeq 0.705$ can be taken to characterize the critical point C_- separating the two stable phases. These properties coincide with those found for $\delta_d < 0$ at the critical point C_+ between the local-moment and ASC_+ phases, and also with those of the asymmetric critical points of the pseudogap Kondo or Anderson models;[14] however, for $r > r^* \simeq \frac{3}{8}$, these properties differ from from those of the corresponding symmetric critical point $\mathrm{C_S}$. (Our observation that the asymmetric critical value of S_{imp} is slightly greater than $\ln 2$ is consistent with Refs. 24 and 25.) For Γ close to Γ_{c1}, the crossover of the thermodynamic properties away from their critical values can be used to define a crossover scale T_1^* that obeys Eq. (38). Table II lists

TABLE II. Exponents describing the local-spin response at the critical points $\mathrm{C}_\pm$ of the particle-hole-asymmetric pseudogap Anderson-Holstein model, evaluated for five band exponents r. The critical exponents are defined in Eqs. (38) and (42). A number in parentheses indicates the estimated random error in the last digit of each exponent.

r	ν_1	β_1	$1/\delta_1$	x_1	γ_1
0.2	6.22(1)	0.15(1)	0.02630(2)	0.9488(2)	5.85(6)
0.3	5.14(1)	0.34(1)	0.07364(1)	0.8629(3)	4.41(3)
0.4	4.29(1)	0.59(1)	0.1569(1)	0.7275(3)	3.12(2)
0.6	1.78(1)	0.188(1)	0.1173(2)	0.7896(4)	1.41(1)
0.8	1.27(1)	0.079(1)	0.0644(5)	0.879(1)	1.10(1)

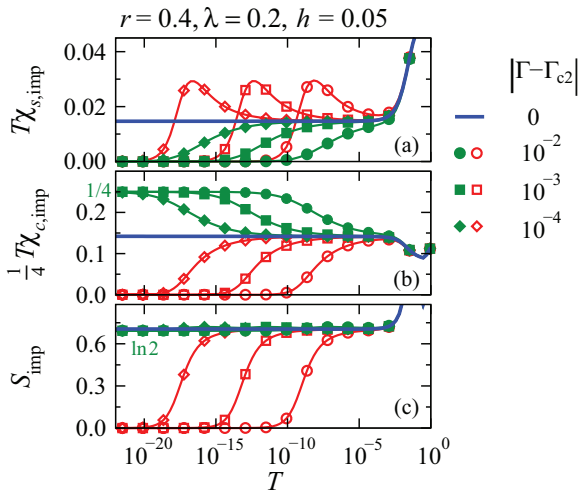

FIG. 14. (Color online) Thermodynamic properties of the particle-hole-symmetric pseudogap Anderson-Holstein model in nonzero local magnetic field near the charge-sector critical point $C_\downarrow$: Temperature dependence of the impurity contribution to (a) the static spin susceptibility $\chi_{s,\mathrm{imp}}$ multiplied by temperature, (b) the static charge susceptibility $T\chi_{c,\mathrm{imp}}$ multiplied by temperature, and (c) the entropy S_{imp}, for $r = 0.4$, $U = -2\varepsilon_d = 0.5$, $h = 0.05$, $\omega_0 = 0.1$, $\lambda = 0.2 > \lambda_0 \simeq 0.158$, and the seven values of $\Gamma - \Gamma_{c2}$ labeled in the legend. Filled (open) symbols connected by guiding lines represent data in the local-charge ($\mathrm{ASC}_\downarrow$) phase, while thick lines without symbols show the critical properties at $C_\downarrow$. $N_s = 3000$ states were retained after each NRG iteration.

the correlation-length exponent $\nu_1(r)$ obtained for five values of r.

2. *Strong bosonic coupling*

Figure 14 plots the temperature dependence of $T\chi_{s,\mathrm{imp}}$, $\frac{1}{4}T\chi_{c,\mathrm{imp}}$, and S_{imp} for $r = 0.4$, $U = -2\varepsilon_d = 0.5$ (i.e., $\delta_d = 0$), $h = 0.05$, $\lambda = 0.2$, and various Γ straddling the critical value Γ_{c2}. Just as was found at particle-hole symmetry, the thermodynamic properties for $\lambda > \lambda_0$ are related to those for $\lambda < \lambda_0$ by interchange of spin and charge degrees of freedom. For the cases shown in Fig. 14, it is the charge susceptibility that most clearly distinguishes the critical point $C_\downarrow$ ($\frac{1}{4}T\chi_{c,\mathrm{imp}} \simeq 0.1419$) from the local-charge and $\mathrm{ASC}_\downarrow$ phases ($\frac{1}{4}T\chi_{c,\mathrm{imp}} = \frac{1}{4}$ and 0, respectively).

C. Local response and universality class

In the vicinity of the quantum-critical points $C_\pm$ separating the local-moment and $\mathrm{ASC}_\pm$ phases, the local-spin responses exhibit power-law behaviors described by Eqs. (38) and (42). Table II lists critical exponents at $C_\pm$ obtained for five different values of r. To within their estimated accuracy, the exponents obey the hyperscaling relations (43), providing evidence for the interacting character of the critical points.

Comparison between Tables I and II shows that the symmetric critical point C_S and its asymmetric counterparts $C_\pm$ have the same low-temperature physics for $r = 0.2$ and 0.3, but not for $r = 0.4$. This pattern is consistent with the pseudogap Kondo model,[14] where the C_S and $C_\pm$ critical points are identical for $0 < r < r^* \simeq \frac{3}{8}$ but distinct for $r^* \lesssim r < 1$. In the latter range, the exponents listed in Table II coincide to within small errors with those for the particle-hole-asymmetric pseudogap Kondo model given in Table II of Ref. 23.

In the vicinity of the critical points $C_{\uparrow,\downarrow}$ marking the transitions from the local-charge phase to the $\mathrm{ASC}_{\uparrow,\downarrow}$ phases, the local charge responses exhibit power-law behaviors described by critical exponents equal (within small errors) to the local-spin exponents of the $C_\pm$ critical points of the pseudogap Kondo and pseudogap Anderson-Holstein models. We are led to conclude that these critical points all lie in the same universality class. Given the different symmetries of the Anderson-Holstein model under spin and isospin rotation, the equivalence of the $C_\pm$ and $C_{\uparrow,\downarrow}$ critical points under spin-charge interchange is a nontrivial finding, distinct from the equivalence of the C_S and C_C critical points at particle-hole symmetry.

V. RESULTS: DOUBLE QUANTUM DOTS WITH $U_2 = 0$

In the pseudogap Kondo and Anderson models, the interacting quantum-critical points found for band exponents $0 < r < 1$ are replaced for $r \geqslant 1$ by first-order QPTs that arise from renormalized level crossings between spin-doublet and spin-singlet ground states of the impurity.[25] Similar behavior is expected in the pseudogap Anderson-Holstein model. This section focuses on the particular case $r = 2$ that is of particular interest because it has a possible realization in double quantum dots. Following, we present results not only for the impurity contributions to thermodynamic properties but also for the linear conductance of such a double-dot system in the vicinity of its spin- and charge-sector QPTs.

A. Pseudogapped effective model for double quantum dots

The motivation for focusing on the case $r = 2$ comes from theoretical studies[20–22] of two lateral quantum dots coupled in parallel to left (L) and right (R) leads, and gated in such a manner that the low-energy physics is dominated by just one single-particle state on each dot. It is assumed that one of the dots (dot 1) is small and hence strongly interacting, while the other (dot 2) is larger, has a negligible charging energy, and can be approximated as a noninteracting resonant level. This setup can be described by the two-impurity Anderson Hamiltonian

$$\hat{H}_{DD} = \sum_{j,\sigma} \varepsilon_j \hat{n}_{j\sigma} + U_1 \hat{n}_{1\uparrow}\hat{n}_{1\downarrow} + \sum_{\ell,\mathbf{k},\sigma} \varepsilon_{\ell\mathbf{k}} c^\dagger_{\ell\mathbf{k}\sigma} c_{\ell\mathbf{k}\sigma} + \sum_{j,\ell,\mathbf{k},\sigma} V_{j\ell}(d^\dagger_{j\sigma} c_{\ell\mathbf{k}\sigma} + \mathrm{H.c.}). \quad (49)$$

Here, $d_{j\sigma}$ annihilates an electron of spin z component σ and energy ε_j in the dot j ($j = 1, 2$), $\hat{n}_{j\sigma} = d^\dagger_{j\sigma} d_{j\sigma}$ is the number operator for such electrons, and $c_{\ell\mathbf{k}\sigma}$ annihilates an electron of spin z component σ and energy $\varepsilon_{\ell\mathbf{k}}$ in lead ℓ ($\ell = L, R$). For simplicity, the leads are assumed to have the same dispersion $\varepsilon_{\ell\mathbf{k}} = \varepsilon_{\mathbf{k}}$ corresponding to a "top-hat" density of states $\rho(\varepsilon) = \rho_0\Theta(D - |\varepsilon|)$ with $\rho_0 = (2D)^{-1}$, and to hybridize symmetrically with the dots so that $V_{jL} = V_{jR}$. Under these conditions, the dots couple only to the symmetric combination of lead electrons annihilated by $c_{\mathbf{k}\sigma} = (c_{L\mathbf{k}\sigma} + c_{R\mathbf{k}\sigma})/\sqrt{2}$ with effective hybridization matrix elements $V_j = \sqrt{2}V_{j\ell}$.

A key feature of Eq. (49) is the vanishing of the dot-2 Coulomb interaction U_2 associated with a Hamiltonian term $U_2\hat{n}_{2\uparrow}\hat{n}_{2\downarrow}$. This allows one to integrate out dot 2 to yield an effective Anderson model for a single impurity characterized by a level energy ε_1, an onsite interaction U_1, and a hybridization function[20]

$$\mathbf{\Gamma}_1(\varepsilon) = \frac{(\varepsilon-\varepsilon_2)^2}{(\varepsilon-\varepsilon_2)^2+\Gamma_2^2}\,\Gamma_1\,\Theta(D-|\varepsilon|), \tag{50}$$

where $\Gamma_j = \pi\rho_0 V_j^2$ for $j = 1, 2$. The presence of dot 2 in the original model manifests itself here as a Lorentzian hole in $\mathbf{\Gamma}_1(\varepsilon)$ of width Γ_2 centered on $\varepsilon = \varepsilon_2$. For $\varepsilon_2 = 0$ (a condition that might be achieved in practice by tuning a plunger gate voltage on dot 2), $\mathbf{\Gamma}_1(\varepsilon) \propto \varepsilon^2$ in the vicinity of the Fermi energy, providing a realization of the $r = 2$ pseudogap Anderson model.[20]

In the remainder of this section, we consider the double-dot device introduced in Ref. 20, augmented by a Holstein coupling between dot 1 and local bosons. Such a system, modeled by a Hamiltonian $\hat{H}_{DD} + \omega_0 a^\dagger a + \lambda(\hat{n}_1 - 1)(a + a^\dagger)$, can be mapped (following Ref. 20) onto the effective single-impurity model

$$\hat{H} = \sum_\sigma \varepsilon_1\hat{n}_1 + U_1\hat{n}_\uparrow\hat{n}_\downarrow + \sum_{\mathbf{k},\sigma}\varepsilon_{\mathbf{k}}c^\dagger_{\mathbf{k}\sigma}c_{\mathbf{k}\sigma} + \omega_0 a^\dagger a + \sum_{\mathbf{k},\sigma} V_1(d^\dagger_\sigma c_{\mathbf{k}\sigma} + \text{H.c.}) + \lambda(\hat{n}_1 - 1)(a + a^\dagger) \tag{51}$$

with the hybridization function $\mathbf{\Gamma}_1(\varepsilon) = \pi N_k^{-1}\sum_{\mathbf{k}} V_1^2\delta(\varepsilon - \varepsilon_{\mathbf{k}})$ as defined in Eq. (50).

All numerical results presented in the remainder of this section were obtained using the effective one-impurity pseudogap Anderson-Holstein model [Eq. (51)] for a strongly interacting dot 1 having $U_1 = 0.5$ and for a bosonic frequency $\omega_0 = 0.1$. The NRG calculations were performed for a discretization parameter $\Lambda = 2.5$.

B. Phase boundaries

1. Weak bosonic coupling

Figure 15(a) shows the phase diagram of the $U_2 = 0$ double-quantum-dot device, as mapped to the pseudogap Anderson-Holstein model, on the λ^2-ε_1 plane in the absence of any magnetic field. For $\lambda < \lambda_0 \simeq 0.158\,284\,8$, decreasing the dot-1 energy starting from a large positive value drives the system from the ASC$_-$ phase to the local-moment phase (LM) at $\varepsilon_1 = \varepsilon^+_{1,c} \leqslant 0$, and then from the local-moment phase to the ASC$_+$ phase at $\varepsilon_1 = \varepsilon^-_{1,c} = -U_1 - \varepsilon^+_{1,c}$. For $\lambda > \lambda_0$, the system instead lies in the ASC$_-$ phase for all $\varepsilon_1 > -\frac{1}{2}U_1$, in the ASC$_+$ phase for all $\varepsilon_1 < -\frac{1}{2}U_1$, and in the local-charge phase (LC) only along the line $\varepsilon_1 = -U_1/2$ of strict particle-hole symmetry.

One of the most notable features of Fig. 15(a) is the linear dependence of $\varepsilon^\pm_{1,c}$ on λ^2, which implies a linear dependence on the polaron energy $\varepsilon_p = \lambda^2/\omega_0$. Since $\varepsilon^-_{1,c} = -U_1 - \varepsilon^+_{1,c}$, it suffices to focus on the phase boundary between the ASC$_-$ and LM phases. In the atomic limit $\Gamma = 0$, one expects this boundary to be defined by the degeneracy of the $n_d = 0$ and 1 impurity levels, i.e., the point where the renormalized

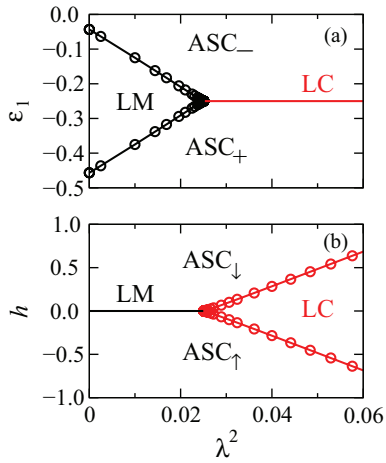

FIG. 15. (Color online) Phase diagrams of a $U_2 = 0$ double-quantum-dot device with $U_1 = 0.5$, $\Gamma_1 = 0.05$, $\varepsilon_2 = 0$, $\Gamma_2 = 0.02$, and $\omega_0 = 0.1$: (a) The λ^2-ε_1 plane for $h = 0$. (b) The λ^2-h plane for $\varepsilon_1 = -\frac{1}{2}U_1$. Note the near linearity of the phase boundaries in each panel when plotted against the square of the bosonic coupling.

dot-1 level energy [cf. Eq. (11)] satisfies $\bar{\varepsilon}_1 \equiv \varepsilon_1 + \varepsilon_p = 0$, a condition that implies $\varepsilon^+_{1,c} = -\varepsilon_p$.

The location of the phase boundary for $\Gamma > 0$ can be estimated using the poor-man's scaling equations discussed in Sec. II C. Equation (21) implies that for $r > 1$, the effective value of the dimensionless scattering width $\tilde{\Gamma}/\tilde{D} = (\tilde{D}/D)^{r-1}(\Gamma/D)$ decreases monotonically under reduction of the half-bandwidth from D to $\tilde{D}$. If $\Gamma < D$, this decrease rules out the possibility of entry into the mixed-valence regime under the criteria laid out at the end of Sec. II C. Moreover, the decrease of $\tilde{\Gamma}$ is so rapid that any entry to the local-moment regime and subsequent mapping to the pseudogap Kondo problem will yield a subcritical exchange coupling, placing the system in the local-moment phase. Under these circumstances, the boundary between the local-moment phase and the asymmetric strong-coupling phase ASC$_-$ [see Sec. II B 1 and in particular Fig. 1(b)] is effectively determined by the condition $\tilde{\varepsilon}_d(\tilde{D} = 0) = 0$ for a level crossing between the renormalized energies of the empty and singly occupied impurity configurations. With the approximation $U = \infty$, and using the expansion

$$S(a,x) \simeq 1 - \frac{x}{a+1} + O(x^2) \quad \text{for} \quad x > 0, \tag{52}$$

Eq. (17) can be integrated to yield

$$\varepsilon^+_{d,c} \simeq -\frac{\Gamma}{2\pi} - \alpha_1\,\varepsilon_p, \tag{53}$$

with

$$\alpha_1 = 1 - \left(1 - \frac{\omega_0}{D}\,\ln\frac{D+\omega_0}{\omega_0}\right)\frac{\Gamma}{\pi D}. \tag{54}$$

The predicted value $\alpha_1 = 0.986$ is in good agreement with the one $\alpha_1 = 0.988$ that describes NRG results for the Anderson-Holstein model with $U = 0.5$, $\Gamma = 0.05$, and a pure $r = 2$ power-law hybridization function (data not shown). The phase boundary for the mapped double-quantum-dot system plotted in Fig. 15(a) can be fitted with a reduced value $\alpha_1 = 0.80$ that can be attributed to the fact that the hybridization function

$\mathbf{\Gamma}_1(\varepsilon)$ in Eq. (50) assumes a power-law form only for $|\varepsilon| \ll \Delta_2 \ll D$.

2. Strong bosonic coupling

Figure 15(b) shows the phase diagram of the $U_2 = 0$ double-quantum-dot system on the λ^2-h plane at particle-hole symmetry. For $\lambda > \lambda_0$, decreasing the local magnetic field from a large positive value takes the system from the $\mathrm{ASC}_\downarrow$ phase to the local-charge phase (LC) at $h = h_c > 0$, and then from the local-charge phase to the $\mathrm{ASC}_\uparrow$ phase at $h = -h_c$. For $\lambda < \lambda_0$, by contrast, the system is in the $\mathrm{ASC}_\downarrow$ or $\mathrm{ASC}_\uparrow$ phase for $h > 0$ or $h < 0$, respectively, and in the local-charge phase only along the line $h = 0$.

The phase boundaries shown in Fig. 15(b) are nearly linear in $\lambda^2 - \lambda_0^2$ or, equivalently, linear in $2\varepsilon_p - U$. In the atomic limit $\Gamma = 0$, one expects the boundary between the $\mathrm{ASC}_\downarrow$ and LC phases to be located at the point where the singly occupied $S_z = -\frac{1}{2}$ impurity state crosses energies with the degenerate pair of impurity states having $n_d = 0, 2$, i.e., to satisfy $-\frac{1}{2}h_c = \frac{1}{2}\bar{U}$ or $h_c = 2\varepsilon_p - U$. For $\Gamma > 0$, a generalization of the poor-man's scaling analysis of Sec. II C to incorporate the local field would be expected to yield corrections to this result along lines similar to the corrections found in the regime $\lambda < \lambda_0$. Empirically, we find that the data in Fig. 15(b) for $0 < \lambda - \lambda_0 \ll \lambda_0$ can be fitted to the form

$$h_c \simeq \alpha_2(2\varepsilon_p - U) \tag{55}$$

with $\alpha_2 = 0.69$. However, a larger value $\alpha_2 \simeq 1$ is required to describe the data points for $\lambda \simeq 2\lambda_0$, indicating that the critical field is not strictly linear in $2\varepsilon_p - U$.

C. Crossover scales

As discussed in Sec. III C, we can use the NRG spectrum to identify temperature scales characterizing crossovers between different renormalization-group fixed points. Figure 16(a) plots the crossover scale T_1^* versus $\Delta\varepsilon_1 = \varepsilon_1 - \varepsilon_{1,c}^+$ on approach to the local-moment phase boundary from the ASC_- phase for a weak bosonic coupling $\lambda = 0.1$, while Fig. 16(b) shows the scale T_2^* versus $\Delta h = h - h_c$ in the $\mathrm{ASC}_\downarrow$ phase near the local-charge phase boundary for $\lambda = 0.2$. T_1^* and T_2^* vanish at the phase boundaries in the manner

$$T_1^* \propto |\varepsilon - \varepsilon_{c1}^+|^{\nu_1} \quad \text{as} \quad \varepsilon \to \varepsilon_{1,c}^+ \tag{56}$$

and

$$T_2^* \propto |h - h_c|^{\nu_2} \quad \text{as} \quad h \to h_c, \tag{57}$$

with correlation-length exponents $\nu_1 = \nu_2 = 1$. This linear vanishing of crossover scales is consistent with the level-crossing nature of the QPTs of the pseudogap Anderson-Holstein model for $r = 2$.

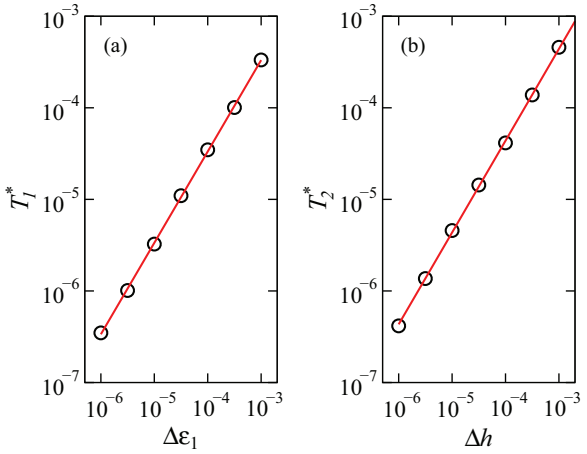

FIG. 16. (Color online) Crossover temperature scales near QPTs in a $U_2 = 0$ double-quantum-dot device with $U_1 = 0.5$, $\Gamma_1 = 0.05$, $\varepsilon_2 = 0$, $\Gamma_2 = 0.02$, and $\omega_0 = 0.1$: (a) T_1^* vs $\Delta\varepsilon_1 = \varepsilon_1 - \varepsilon_{1,c}^+$ in the ASC_- phase for $h = 0$ and $\lambda = 0.1$. (b) T_2^* vs $\Delta h = h - h_c$ in the $\mathrm{ASC}_\downarrow$ phase for $\varepsilon_1 = -0.25$ and $\lambda = 0.2$. Straight lines represent power-law fits, which yield the correlation-length exponents $\nu_1 = \nu_2 = 1$. $N_s = 1000$ states were retained after each NRG iteration.

D. Impurity thermodynamic properties

As in the cases $r < 1$ considered above, the temperature variation of the impurity contributions[56] to the static spin and charge susceptibilities and to the entropy can be used to distinguish the strong-coupling phases of the $U_2 = 0$ double-quantum-dot system from the phases with residual local spin or charge degrees of freedom.

1. Weak bosonic coupling

Figure 17 plots the temperature dependence of the impurity thermodynamic properties $T\chi_{s,\mathrm{imp}}$, $\frac{1}{4}T\chi_{c,\mathrm{imp}}$, and S_{imp} for $h = 0$, a weak bosonic coupling $\lambda = 0.1$, and various values of ε_1 straddling the upper transition. For $\varepsilon_1 = \varepsilon_{1,c}^+ \simeq -0.124\,985$ (lines without symbols in Fig. 17), the low-temperature limiting values $T\chi_{s,\mathrm{imp}} = \frac{1}{6}$, $\frac{1}{4}T\chi_{c,\mathrm{imp}} = \frac{1}{18}$, and $S_{\mathrm{imp}} = \ln 3$

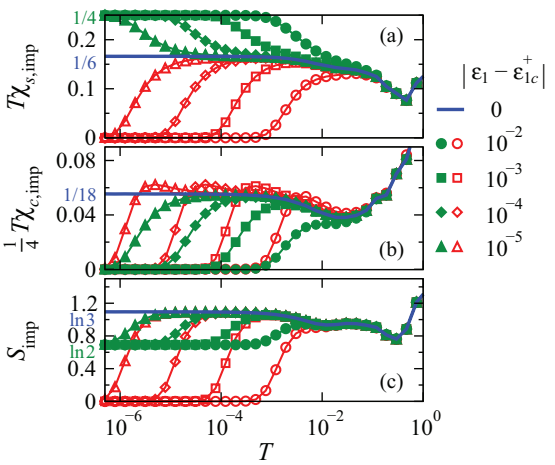

FIG. 17. (Color online) Thermodynamic properties of a $U_2 = 0$ double-quantum-dot device near a spin-sector QPT: Temperature dependence of the impurity contribution to (a) the static spin susceptibility $\chi_{s,\mathrm{imp}}$ multiplied by temperature, (b) the static charge susceptibility $\chi_{c,\mathrm{imp}}$ multiplied by temperature, and (c) the entropy S_{imp}, for $U_1 = 0.5$, $\Gamma_1 = 0.05$, $\varepsilon_2 = 0$, $\Gamma_2 = 0.02$, $h = 0$, $\omega_0 = 0.1$, $\lambda = 0.1$, and nine values of $|\varepsilon_1 - \varepsilon_{1,c}^+|$ where $\varepsilon_{1,c}^+ \simeq -0.124\,985$. Properties at the transition (thick lines without symbols) are those expected at a level crossing between the local-moment phase (filled symbols) and the ASC_- phase. $N_s = 3000$ states were retained after each NRG iteration.

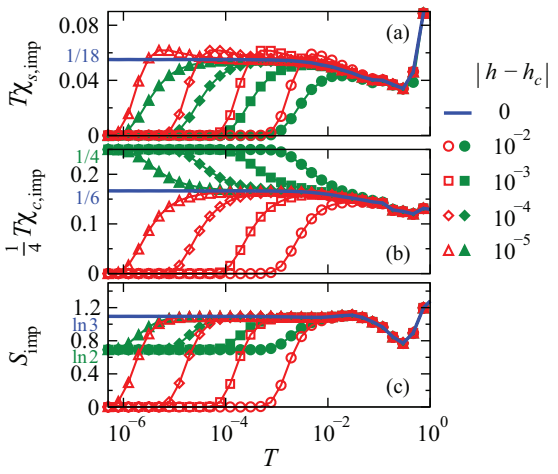

FIG. 18. (Color online) Thermodynamic properties of a $U_2 = 0$ double-quantum-dot device near a charge-sector QPT: Temperature dependence of the impurity contribution to (a) the static spin susceptibility $\chi_{s,\mathrm{imp}}$ multiplied by temperature, (b) the static charge susceptibility $\chi_{c,\mathrm{imp}}$ multiplied by temperature, and (c) the entropy S_{imp}, for $U_1 = -2\varepsilon_1 = 0.5$, $\Gamma_1 = 0.05$, $\varepsilon_2 = 0$, $\Gamma_2 = 0.02$, $\omega_0 = 0.1$, $\lambda = 0.2$, and nine values of $|h - h_c|$ where $h_c \simeq 0.284\,959$. Properties at the transition (thick lines without symbols) are those expected at a level crossing between the local-charge phase (filled symbols) and the ASC$_\downarrow$ phase. $N_s = 3000$ states were retained after each NRG iteration.

are those characteristic of the *valence-fluctuation* fixed point: the point of degeneracy between impurity occupancies $n_d = 0$ and 1 corresponding to Eq. (51) with effective couplings $\varepsilon_1 = \Gamma_1 = \lambda = 0$ and $U_1 = \infty$. If ε_1 deviates slightly from its critical value, the properties trace their critical behaviors at high temperatures, but cross over below a scale T_1^* to those either of the local-moment phase, where there is a residual spin-$\frac{1}{2}$ degree of freedom ($T\chi_{s,\mathrm{imp}} = \frac{1}{4}$, $T\chi_{c,\mathrm{imp}} = 0$, and $S_{\mathrm{imp}} = \ln 2$) or of the ASC$_-$ phase ($T\chi_{s,\mathrm{imp}} = T\chi_{c,\mathrm{imp}} = S_{\mathrm{imp}} = 0$).

2. Strong bosonic coupling

Figure 18 shows $T\chi_{s,\mathrm{imp}}$, $\frac{1}{4}T\chi_{c,\mathrm{imp}}$, and S_{imp} versus T at particle-hole symmetry ($\varepsilon_1 = -\frac{1}{2}U_1$) for a strong bosonic coupling $\lambda = 0.2$ and various local magnetic fields h straddling the critical value $h_c \simeq 0.284\,959$. Here, in contrast to Fig. 17, $T\chi_{s,\mathrm{imp}}$ falls to zero in both the local-charge phase and the ASC$_\downarrow$ phase, signaling the suppression of spin fluctuations at the impurity site. However, the flows of $T\chi_{c,\mathrm{imp}}$ with decreasing temperature clearly reveal the existence of a QPT separating the ASC$_\downarrow$ and local-charge phases. Exactly at the critical value $h = h_c$ (lines without symbols in Fig. 18), $\frac{1}{4}T\chi_{c,\mathrm{imp}}$ is pinned at low temperatures at the value $\frac{1}{6}$ expected at the point of degeneracy between the empty, spin-down, and doubly occupied impurity configurations. For h deviating slightly from h_c, $T\chi_{c,\mathrm{imp}}$ traces the critical behavior at high temperatures but eventually crosses below a scale T_2^* to a limiting value of either 1 in the local-charge phase or 0 in the ASC$_\downarrow$ phase.

The temperature dependence of the spin (charge) susceptibility in Fig. 18 mirrors that of the charge (spin) susceptibility in Fig. 17. By contrast, the behavior of $S_{\mathrm{imp}}(T)$ is equivalent in the two cases. These properties suggest that, as found for the interacting quantum-critical points for band exponents $0 < r < 1$ (Secs. III and IV), the quantum phase transitions into/out of the LC phase at $\delta_d = 0$ take place at points of enhanced symmetry where the system acquires an SU(2) isospin invariance to match the global SU(2) spin invariance of the Anderson-Holstein Hamiltonian in zero magnetic field.

Both at weak and strong bosonic couplings, the fact that the impurity properties in the quantum-critical regime are those of the valence-fluctuation fixed point (or its analog under interchange of spin and isospin) is entirely consistent with the picture of each QPT as arising from a renormalized level crossing. Moreover, crossover scales T_1^* and T_2^* extracted from the thermodynamic properties are identical up to a constant multiplicative factor to those identified from the NRG spectra (see Sec. V C).

E. Linear conductance

It is generally impractical to measure the impurity thermodynamic properties of a quantum-dot device. Rather, the primary experimental probe of lateral quantum dots is electrical transport. The linear conductance of the boson-coupled double-quantum-dot system modeled by Eq. (49) can be calculated from the Landauer formula

$$g(T) = \frac{e^2}{h}\sum_\sigma \int_{-\infty}^{\infty} d\omega\,(-\partial f/\partial\omega)[-\mathrm{Im}\mathcal{T}_\sigma(\omega)], \qquad (58)$$

where $f(\omega,T) = [\exp(\omega/T)+1]^{-1}$ is the Fermi-Dirac distribution function and $\mathcal{T}_\sigma(\omega) = \pi\rho_0 \sum_{i,j} V_i\, G^\sigma_{ij}(\omega)\, V_j$ with $G^\sigma_{ij}(\omega) = -i\int_0^\infty dt\, e^{i\omega t}\langle\{d_{i\sigma}(t), d^\dagger_{j\sigma}(0)\}\rangle$. For $U_2 = 0$, one can reexpress[21]

$$-\mathrm{Im}\,\mathcal{T}_\sigma(\omega) = [1 - 2\pi\Gamma_2\rho_2(\omega)]\pi\mathbf{\Gamma}(\omega)A^\sigma_{11}(\omega) + \pi\Gamma_2\rho_2(\omega) + 2\pi(\omega-\varepsilon_2)\mathbf{\Gamma}(\omega)\rho_2(\omega)\,\mathrm{Re}\,G^\sigma_{11}(\omega), \qquad (59)$$

where $\mathbf{\Gamma}(\omega)$ is as defined in Eq. (50), $\rho_2(\varepsilon) = (\Gamma_2/\pi)[(\varepsilon - \varepsilon_2)^2 + \Gamma_2^2]^{-1}$ is a Lorentzian of width Γ_2 centered on energy ε_2, and $A^\sigma_{11}(\omega) = -\pi^{-1}\mathrm{Im}\,G^\sigma_{11}(\omega)$. All quantities entering Eq. (58) are known exactly with the sole exception of $G^\sigma_{11}(\omega)$, the full dot-1 spin-σ local Green's function $G^\sigma_{11}(\omega)$ taking into account both electron-electron (U_1) and electron-boson (λ) coupling.

We have used standard NRG methods[65] to obtain the dot-1 spectral function $A^\sigma_{11}(\omega)$ from the effective one-impurity pseudogap Anderson-Holstein model described by Eq. (51). After $\mathrm{Re}\,G^\sigma_{11}(\omega)$ has been obtained via the Kramers-Kronig relations, Eqs. (58) and (59) yield the linear conductance. We present results only for zero magnetic field [where $A^\uparrow_{11}(\omega) = A^\downarrow_{11}(\omega)$] and/or for strict particle-hole symmetry [where $A^\uparrow_{11}(\omega) = A^\downarrow_{11}(-\omega)$], special cases in which the up- and down-spin channels contribute equally to the conductance. Temperatures are expressed as multiples of $T_{K0} = 7\times10^{-4}$, the Kondo temperature for the conventional (i.e., metallic or $r = 0$) one-impurity Anderson model with $U = -2\varepsilon_d = 0.5$ and $\Gamma = 0.05$, which serves as a characteristic scale for the many-body physics of the problem.

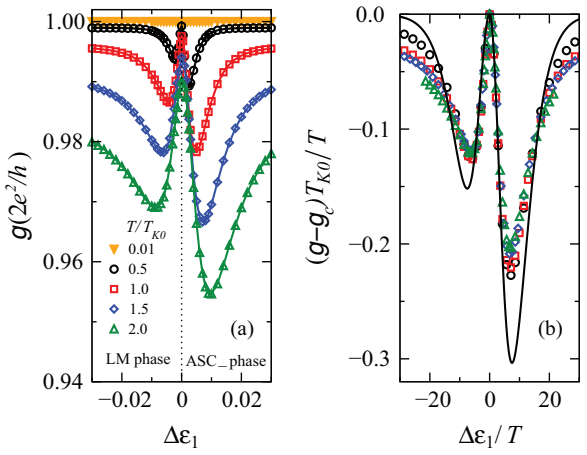

FIG. 19. (Color online) Linear conductance of a $U_2 = 0$ double-quantum-dot device near a spin-sector QPT: (a) Linear conductance g vs $\Delta\varepsilon_1 = \varepsilon_1 - \varepsilon^+_{1,c}$ for $U_1 = 0.5$, $\Gamma_1 = 0.05$, $\varepsilon_2 = 0$, $\Gamma_2 = 0.02$, $h = 0$, $\omega_0 = 0.1$, $\lambda = 0.1$, and different temperatures T specified in the legend as multiples of $T_{K0} = 7 \times 10^{-4}$. The retention of $N_s = 1000$ states after each NRG iteration accounts for the small discrepancy between $\varepsilon^+_{1,c} \simeq -0.124\,987\,1$ and its value in the case $N_s = 3000$ shown in Fig. 17. (b) The same data scaled as $(g - g_c)T_{K0}/T$ vs $\Delta\varepsilon_1/T$, where $g_c(T)$ is the conductance at $\varepsilon_1 = \varepsilon^+_{1,c}$. The solid line was obtained from Eq. (62) by approximating $A_q(x) = a_q$ and using values of a_q and $\omega_q/(\varepsilon_1 - \varepsilon^+_1)$ fitted from $A^\sigma_{11}(\omega)$.

1. Weak bosonic coupling

Figure 19(a) plots g versus $\Delta\varepsilon_1 = \varepsilon_1 - \varepsilon^+_{1,c}$ for a weak bosonic coupling $\lambda = 0.1$ and five temperatures T listed in the legend. At $T = 0$, the linear conductance g is structureless and takes its maximum possible value $2e^2/h$, signaling perfect electron transaction through the system. However, at $T > 0$, g versus $\Delta\varepsilon_1$ develops clear minima on either side of a maximum located precisely on the boundary $\Delta\varepsilon_1 = 0$ between the local-moment and ASC$_-$ phases. The peak-and-valley structure becomes more prominent upon increasing temperature up to several times T_{K0}, making it amenable to experimental observation. Similar features have been reported [see Fig. 2(b) of Ref. 21] for a double-quantum-dot system without bosonic coupling.

The essential features of the results shown in Fig. 19(a) can be understood from the fact that, just as in the case of zero bosonic coupling,[21] near the QPT, the low-energy part of the dot-1 spectral function is dominated at low temperatures by a quasiparticle peak at frequency $\omega_q \propto \varepsilon_1 - \varepsilon^+_1$. Upon raising the temperature, this peak rapidly disappears once $T \gtrsim \omega_q$. We approximate this behavior by

$$A^\sigma_{11}(\omega) \simeq A_q(\omega_q/T)\,\delta(\omega - \omega_q) \quad \text{for} \quad |\omega| \ll \Gamma_2, \tag{60}$$

where $A_q(x)$ is an unknown scaling function that satisfies $A_q(x) \to 0$ for $x \ll 1$ and $A_q(x) \to a_q > 0$ for $x \gg 1$. Hilbert transformation of Eq. (60) leads to

$$\mathrm{Re}\, G^\sigma_{11}(\omega,T) \simeq R_0(\omega_q,T) + R_1(\omega_q,T)\,\frac{\omega}{\Gamma_2} + \frac{A_q(\omega_q/T)}{\omega_q - \omega}, \tag{61}$$

where R_0 and R_1 are determined by the form of $A^\sigma_{11}(\omega)$ at $|\omega| \gtrsim \Gamma_2$, and may vary with ε_1 and hence ω_q. Inserting Eqs. (60) and (61) into Eqs. (58) and (59) yields, for $\varepsilon_2 = 0$ and $T \ll \Gamma_2$,

$$g = \frac{2e^2}{h}\left\{1 - \frac{\pi^2}{3}\left(\frac{T}{\Gamma_2}\right)^2 - A_q(\omega_q/T)\,\frac{\Gamma_1 T}{\Gamma_2^2}\left[\frac{\pi(\omega_q/T)^2\, e^{\omega_q/T}}{(e^{\omega_q/T}+1)^2} + \frac{4T}{\Gamma_2}\int_0^\infty dx\,\frac{x^4}{x^2 - (\omega_q/T)^2}\,\frac{e^x}{(e^x+1)^2}\right] + O\left(\frac{T}{\Gamma_2}\right)^4\right\}. \tag{62}$$

The first line in Eq. (62), which describes resonant tunneling through dot 2, dominates the conductance both for $T \ll \omega_q$ and for $T \gg \omega_q$. However, for $T \simeq \omega_q$, the conductance is dominated by the first term in the square brackets, which arises from the A^σ_{11} term in Eq. (59). To good approximation, the conductance near the QPT (where $\omega_q = 0$) can be expressed as

$$g(\varepsilon_1,T) = g(\varepsilon^+_{1,c},T) + T\, g_1\left(\frac{\varepsilon_1 - \varepsilon^+_{1,c}}{T}\right) \tag{63}$$

with $g_1(0) = 0$. Figure 19(b) shows that this form is obeyed well by the NRG results. The precise scaling function g_1 can not be determined without knowledge of $A_q(x)$, but the zeroth-order approximation $A_q(x) = a_q$ produces a reasonably good description of the numerical data. This scaling collapse of the finite-temperature conductance feature provides a clear signature of the underlying $T = 0$ phase transition that may be sought in experiments.

2. Strong bosonic coupling

As one would expect given the equivalence under spin-charge interchange of the thermodynamic properties at the LM-ASC$_\pm$ and LC-ASC$_{\uparrow,\downarrow}$ phase boundaries, the variation of the conductance with h around the critical field h_c for $\lambda > \lambda_0$ is very similar to the variation of g with ε_1 near $\varepsilon^\pm_{1c}$. The system exhibits perfect electron transmission ($g = 2e^2/h$) at $T = 0$ and with increasing temperature develops an increasingly prominent peak-and-valley signature of the QPT. This signature can be understood as arising from the existence of quasiparticle peaks $A^\uparrow_{11}(\omega) \simeq A_q(\omega_q/T)\,\delta(\omega - \omega_q)$ and $A^\downarrow_{11}(\omega) \simeq A_q(\omega_q/T)\,\delta(\omega + \omega_q)$ at a frequency $\omega_q \propto h - h_c$. Analysis similar to that applied in the case of weak bosonic couplings leads to the prediction

$$g(h,T) = g(h_c,T) + T\,\tilde{g}_1\left(\frac{h - h_c}{T}\right), \tag{64}$$

a scaling that is indeed displayed by the numerical data. (We do not show these data explicitly due to their similarity with Fig. 19.)

VI. SUMMARY

We have conducted a study of the pseudogap Anderson-Holstein model describing a magnetic impurity level that hybridizes with a pseudogapped fermionic host with a density of states vanishing as $|\varepsilon|^r$ at the Fermi energy ($\varepsilon = 0$), and that is also coupled, via its charge, to a local-boson mode. The reduction of the density of low-energy band excitations leads to quantum phase transitions (QPTs) that can be classified into different types depending on the strength of the impurity-boson

coupling and on the presence or absence of particle-hole and time-reversal symmetry. The main results are as follows:

(1) Under conditions of strict particle-hole and time-reversal symmetry, the pseudogap Anderson-Holstein model with exponent $0 < r < \frac{1}{2}$ features two types of continuous QPT. For a weak (strong) impurity-boson coupling that results in a positive (negative) effective Coulomb interaction between electrons in the impurity level, increasing the impurity-band hybridization from zero drives the system through a continuous QPT between a local-moment (local-charge) phase, in which a twofold degree of freedom survives to $T = 0$, and a symmetric strong-coupling phase in which the impurity degree of freedom is quenched by the conduction band. Critical exponents characterizing the response to a local symmetry-breaking field suggest that these QPTs belong to the same universality class as the QPT of the particle-hole-symmetric pseudogap Anderson model.

(2) For $r \geqslant \frac{1}{2}$, the symmetric strong-coupling fixed point is unstable (just as in the pseudogap Anderson model without bosons) and for weak (strong) impurity-boson couplings, a system exhibiting particle-hole and time-reversal symmetry always lies in the local-moment (local-charge) phase.

(3) For weak impurity-boson couplings and away from particle-hole symmetry, the symmetric strong-coupling phase is replaced by two asymmetric strong-coupling phases, one corresponding to an empty impurity level and the other to double occupation of the impurity site. These phases are separated from the local-moment phase by QPTs in the same universality class as those of the particle-hole-asymmetric pseudogap Anderson model. These QPTs are continuous and interacting for $0 < r < 1$, but first order for $r \geqslant 1$.

(4) For strong impurity-boson couplings and in the presence of a magnetic field, the local-charge phase is separated by QPTs (again in the asymmetric pseudogap Anderson universality class, and continuous for $r < 1$ but first order for $r \geqslant 1$) from two asymmetric strong-coupling phases corresponding to single occupation of the impurity level with either a spin-up or a spin-down electron.

(5) For $r = 2$, the pseudogap Anderson-Holstein model provides a description of two quantum dots connected in parallel to current leads, where one dot is tuned to lie in a Coulomb blockade valley and is coupled via its charge to a local-boson mode, while the other dot is tuned to be effectively noninteracting and in resonance with the leads. The setup exhibits voltage- or magnetic-field-tuned QPTs of the level-crossing type. These QPTs produce peak-and-valley features in the linear conductance that become more prominent upon increase of the temperature. Moreover, in the vicinity of the transitions, the conductance data collapse to a single function of the ratio of a symmetry-breaking field to the absolute temperature.

ACKNOWLEDGMENTS

We thank L. G. G. V. Dias da Silva for valuable discussions. Much of the computational work was performed at the University of Florida High-Performance Computing Center. This work was supported in part by NSF Grants No. DMR-0710540 and No. DMR-1107814.

APPENDIX : DERIVATION OF POOR-MAN'S SCALING EQUATIONS

In this Appendix, we outline the derivation of the poor-man's scaling equations (16)–(18) discussed in Sec. II C. For this purpose, it proves convenient to work with the Anderson-Holstein Hamiltonian in the form

$$\hat{H}' = \hat{H}'_{\rm imp} + \hat{H}_{\rm band} + \hat{H}_{\rm boson} + \hat{H}'_{\text{imp-band}} + \hat{H}_{\text{imp-boson}}\,, \tag{A1}$$

where $\hat{H}_{\rm band}$, $\hat{H}_{\rm boson}$, and $\hat{H}_{\text{imp-boson}}$ are as defined in Eqs. (2b), (2c), and (2e), respectively, but $\hat{H}_{\rm imp}$ in Eq. (2a) is rewritten in more conventional fashion as

$$\hat{H}'_{\rm imp} = \varepsilon_d\, n_d + U \hat{n}_{d\uparrow}\hat{n}_{d\downarrow} \tag{A2}$$

and $\hat{H}_{\text{imp-band}}$ in Eq. (2d) is generalized to

$$H'_{\text{imp-band}} = \frac{1}{\sqrt{N_k}} \sum_{\mathbf{k},\sigma} \{[V_{0,\mathbf{k}}(1-\hat{n}_{d,-\sigma}) + V_{2,\mathbf{k}}\,\hat{n}_{d,-\sigma}] d^\dagger_\sigma c_{\mathbf{k}\sigma} + \text{H.c.}\}, \tag{A3}$$

where the hybridization functions

$$\mathbf{\Gamma}_\tau(\varepsilon) = \frac{\pi}{N_k} \sum_{\mathbf{k}} |V_{\tau,\mathbf{k}}|^2 \delta(\varepsilon - \varepsilon_{\mathbf{k}}) = \Gamma_\tau |\varepsilon/D|^r\, \Theta(D - |\varepsilon|) \tag{A4}$$

for $\tau = 0$, 2 have the same power-law dependence as $\mathbf{\Gamma}(\varepsilon)$ defined in Eq. (4). At the bare Hamiltonian level, one expects the hybridization matrix element $V_{0,\mathbf{k}}$ between the empty and singly occupied impurity configurations to be identical to that $V_{2,\mathbf{k}}$ between the singly occupied and doubly occupied impurity configurations. However, this degeneracy can be broken under the scaling procedure.

A canonical transformation $\hat{H}' \to \bar{H}' = e^S \hat{H}' e^{-S}$ with S as defined in Eq. (7) yields

$$\bar{H}' = \bar{H}'_{\rm imp} + \hat{H}_{\rm band} + \hat{H}_{\rm boson} + \bar{H}'_{\text{imp-band}}\,, \tag{A5}$$

where $\bar{H}'_{\rm imp}$ contains shifted parameters $\bar{U}$ [Eq. (9)] and $\bar{\varepsilon}_d$ [Eq. (11)], and

$$\bar{H}'_{\text{imp-band}} = \frac{1}{\sqrt{N_k}} \sum_{\mathbf{k},\sigma} \{B^\dagger [V_{0,\mathbf{k}}(1-\hat{n}_{d,-\sigma}) + V_{2,\mathbf{k}}\,\hat{n}_{d,-\sigma}] d^\dagger_\sigma c_{\mathbf{k}\sigma} + \text{H.c.}\}, \tag{A6}$$

with B as defined in Eq. (13).

We analyze the problem using a basis of many-body states composed as direct products of (i) fermionic states formed by the action of creation and annihilation operators on $|\text{FS}\rangle$, the half-filled Fermi sea having N_k electrons of energy $\varepsilon_{\mathbf{k}} < 0$, and (ii) occupation number eigenstates $|n\rangle$ of the transformed boson mode defined in Eq. (14). Since real occupation of states $|n\rangle$ with $n > 0$ is negligible in the antiadibatic regime, we focus on the states $|0,0\rangle = |\text{FS}\rangle \otimes |0\rangle$, $|\sigma,0\rangle = d^\dagger_\sigma |0,0\rangle$, and $|2,0\rangle = \sigma\, d^\dagger_\sigma |-\sigma,0\rangle$. Neglecting for the moment the effect of the hybridization [$\bar{H}'_{\text{imp-band}}$ in Eq. (A6)], the energies of these states are denoted E_0, $E_1 = E_0 + \bar{\varepsilon}_d$, and $E_2 = E_1 + \bar{\varepsilon}_d + \bar{U} = 2E_1 - E_0 + \bar{U}$.

We now consider the effect of an infinitesimal reduction in the half-bandwidth from D to $\tilde{D} = D + dD$, where $dD < 0$.

The goal is to write a new Hamiltonian $\tilde{H}'$ similar in form to $\bar{H}'$ but retaining only conduction-band degrees of freedom having energies $|\varepsilon_{\mathbf{k}}| < \tilde{D}$ and having parameters $\tilde{\varepsilon}_d$, $\tilde{U}$, and $\tilde{\Gamma}_\tau$ adjusted to account perturbatively for the band-edge states that have been eliminated.

Let K^+ be the set of wave vectors $\mathbf{k}$ describing particlelike states having energies $\tilde{D} < \varepsilon_{\mathbf{k}} < D$, and K^- be the set of wave vectors describing holelike state with energies $-D < \varepsilon_{\mathbf{k}} < -\tilde{D}$. Tunneling of an electron from a K^- state into the empty impurity level, accompanied by the creation of $n = 0, 1, \ldots$ local bosons, transforms the state $|0,0\rangle$ to

$$|\widetilde{0,0}\rangle = |0,0\rangle - \frac{e^{-\lambda^2/2\omega_0^2}}{\sqrt{N_k}} \sum_{\mathbf{k}\in K^-,\,\sigma} V_{0,\mathbf{k}} \times \sum_{n=0}^{\infty} \frac{1}{\sqrt{n!}} \frac{(\lambda/\omega_0)^n}{|\varepsilon_{\mathbf{k}}| + E_1 - E_0 + n\omega_0} c_{\mathbf{k}\sigma}|\sigma,n\rangle + O(V^2) \tag{A7}$$

with energy

$$\tilde{E}_0 = E_0 - \frac{e^{-\lambda^2/\omega_0^2}}{N_k} \sum_{\mathbf{k}\in K^-,\,\sigma} |V_{0,\mathbf{k}}|^2 \times \sum_{n=0}^{\infty} \frac{1}{n!} \frac{(\lambda/\omega_0)^{2n}}{|\varepsilon_{\mathbf{k}}| + E_1 - E_0 + n\omega_0} + O(V^3). \tag{A8}$$

Here, $O(V^m)$ schematically represents all processes involving at least m factors $V_{\tau_1,\mathbf{k}_1}, \ldots, V_{\tau_n,\mathbf{k}_n}$. The derivation of Eqs. (A7) and (A8) makes use of

$$(n|e^{\pm\alpha(b^\dagger - b)}|0) = (n|e^{\pm\alpha(\bar{b}^\dagger - \bar{b})}|0) = e^{-\alpha^2/2}\,(n|e^{\pm\alpha\bar{b}^\dagger} e^{\mp\alpha\bar{b}}|0) = \frac{e^{-\alpha^2/2}}{\sqrt{n!}}\,(\pm\alpha)^n. \tag{A9}$$

Since $N_k^{-1} \sum_{\mathbf{k}\in K^\pm} V_{\tau,\mathbf{k}}^2 \simeq \pi^{-1}\mathbf{\Gamma}_\tau(\pm D)\,\delta(\varepsilon_{\mathbf{k}} \mp D)$, one can reexpress the perturbed energy

$$\tilde{E}_0 \simeq E_0 - |dD|\,\frac{2\mathbf{\Gamma}_0(-D)}{\pi\,\mathcal{E}(D + \bar{\varepsilon}_d)} + O(V^3), \tag{A10}$$

where $\mathcal{E}(E)$ is the energy function defined in Eq. (19).

Similarly, tunneling of an electron from the doubly occupied impurity level into a K^+ state transforms $|2,0\rangle$ to

$$|\widetilde{2,0}\rangle = |2,0\rangle - \frac{e^{-\lambda^2/2\omega_0^2}}{\sqrt{N_k}} \sum_{\mathbf{k}\in K^+,\,\sigma} V_{2,\mathbf{k}} \times \sum_{n=0}^{\infty} \frac{1}{\sqrt{n!}} \frac{(\lambda/\omega_0)^n}{\varepsilon_{\mathbf{k}} - \bar{U} - \bar{\varepsilon}_d + n\omega_0} c_{\mathbf{k}\sigma}^\dagger|-\sigma,n\rangle + O(V^2) \tag{A11}$$

with energy

$$\tilde{E}_2 = E_2 - \frac{e^{-\lambda^2/\omega_0^2}}{N_k} \sum_{\mathbf{k}\in K^+,\,\sigma} |V_{2,\mathbf{k}}|^2 \times \sum_{n=0}^{\infty} \frac{1}{n!} \frac{(\lambda/\omega_0)^{2n}}{\varepsilon_{\mathbf{k}} - \bar{U} - \bar{\varepsilon}_d + n\omega_0} + O(V^3) \simeq E_2 - |dD|\,\frac{2\mathbf{\Gamma}_2(D)}{\pi\,\mathcal{E}(D - \bar{U} - \bar{\varepsilon}_d)} + O(V^3). \tag{A12}$$

Finally, tunneling of an electron into the singly occupied impurity from a K^- state or from the singly occupied level into a K^+ state transforms $|\sigma,0\rangle$ to

$$|\widetilde{\sigma,0}\rangle = |\sigma,0\rangle - \frac{e^{-\lambda^2/2\omega_0^2}}{\sqrt{N_k}} \Bigg[\sum_{\mathbf{k}\in K^-} V_{2,\mathbf{k}} \sum_{n=0}^{\infty} \frac{1}{\sqrt{n!}} \times \frac{(\lambda/\omega_0)^n}{|\varepsilon_{\mathbf{k}}| + E_2 - E_1 + n\omega_0} c_{\mathbf{k},-\sigma}|2,n\rangle - \sum_{\mathbf{k}\in K^+} V_{0,\mathbf{k}} \times \sum_{n=0}^{\infty} \frac{1}{\sqrt{n!}} \frac{(\lambda/\omega_0)^n}{\varepsilon_{\mathbf{k}} + E_0 - E_1 + n\omega_0} c_{\mathbf{k}\sigma}^\dagger|0,n\rangle \Bigg] + O(V^3) \tag{A13}$$

with energy

$$\tilde{E}_1 = E_1 - \frac{e^{-\lambda^2/\omega_0^2}}{N_k} \Bigg[\sum_{\mathbf{k}\in K^-} |V_{2,\mathbf{k}}|^2 \times \sum_{n=0}^{\infty} \frac{1}{n!} \frac{(\lambda/\omega_0)^{2n}}{|\varepsilon_{\mathbf{k}}| + E_2 - E_1 + n\omega_0} - \sum_{\mathbf{k}\in K^+} |V_{0,\mathbf{k}}|^2 \sum_{n=0}^{\infty} \frac{1}{n!} \frac{(\lambda/\omega_0)^{2n}}{\varepsilon_{\mathbf{k}} + E_0 - E_1 + n\omega_0} \Bigg] + O(V^3) \simeq E_1 - |dD| \left[\frac{\mathbf{\Gamma}_2(-D)}{\pi\,\mathcal{E}(D + \bar{U} + \bar{\varepsilon}_d)} + \frac{\mathbf{\Gamma}_0(D)}{\pi\,\mathcal{E}(D - \bar{\varepsilon}_d)} \right] + O(V^3). \tag{A14}$$

The $O(V^2)$ terms in each of the above states $|\widetilde{\phi,0}\rangle$ include terms to enforce normalization, i.e., $\langle\widetilde{\phi,0}|\widetilde{\phi,0}\rangle = \langle\phi,0|\phi,0\rangle = 1$.

The modified energies can be used to define effective Hamiltonian parameters $\tilde{\varepsilon}_d = \tilde{E}_1 - \tilde{E}_0$ and $\tilde{U} = \tilde{E}_2 + \tilde{E}_0 - 2\tilde{E}_1$. At the same time, for each $\mathbf{k}$ in the retained portion of the band (i.e., satisfying $|\varepsilon_{\mathbf{k}}| < \tilde{D}$), $V_{0,\mathbf{k}}$ must be replaced by

$$\tilde{V}_{0,\mathbf{k}} = \begin{cases} \sqrt{N_k}\,\langle\widetilde{0,0}|B^\dagger c_{\mathbf{k}\sigma}\hat{H}'|\widetilde{\sigma,0}\rangle & \text{for } \varepsilon_{\mathbf{k}} > 0, \\ -\sqrt{N_k}\,\langle\widetilde{\sigma,0}|B c_{\mathbf{k}\sigma}^\dagger\hat{H}'|\widetilde{0,0}\rangle & \text{for } \varepsilon_{\mathbf{k}} < 0, \end{cases} \tag{A15}$$

and $V_{2,\mathbf{k}}$ must be replaced by

$$\tilde{V}_{2,\mathbf{k}} = \begin{cases} -\sigma\sqrt{N_k}\,\langle\widetilde{\sigma,0}|B^\dagger c_{\mathbf{k},-\sigma}\hat{H}'|\widetilde{2,0}\rangle & \text{for } \varepsilon_{\mathbf{k}} > 0, \\ \sigma\sqrt{N_k}\,\langle\widetilde{2,0}|B c_{\mathbf{k},-\sigma}^\dagger\hat{H}'|\widetilde{\sigma,0}\rangle & \text{for } \varepsilon_{\mathbf{k}} < 0. \end{cases} \tag{A16}$$

It is straightforward to show that

$$\tilde{V}_{\tau,\mathbf{k}} = V_{\tau,\mathbf{k}} + O(V^3). \tag{A17}$$

We shall not attempt to evaluate the leading corrections, which turn out to be negligible in pseudogap ($r > 0$) cases.

The infinitesimal band-edge reduction described in the previous paragraphs can be carried out repeatedly to reduce the half-bandwidth by a finite amount from D to $\tilde{D} < D$. Equations (A10) and (A14) indicate that during this process, the impurity level energy evolves according to the scaling equation

$$\frac{d\tilde{\varepsilon}_d}{d\tilde{D}} = \frac{1}{\pi}\left[\frac{\tilde{\Gamma}_{0,+}}{\mathcal{E}(\tilde{D} - \tilde{\varepsilon}_d)} - \frac{2\tilde{\Gamma}_{0,-}}{\mathcal{E}(\tilde{D} + \tilde{\varepsilon}_d)} + \frac{\tilde{\Gamma}_{2,-}}{\mathcal{E}(\tilde{D} + \tilde{U} + \tilde{\varepsilon}_d)} \right] + O(V^3), \tag{A18}$$

where $\tilde{\Gamma}_{\tau,\pm}$ is the value of the rescaled hybridization function at the reduced band edges $\varepsilon = \pm\tilde{D}$. Taking into account Eq. (A12) as well, one sees that the onsite repulsion follows:

$$\frac{d\tilde{U}}{d\tilde{D}} = \frac{2}{\pi}\left[\frac{\tilde{\Gamma}_{0,+}}{\mathcal{E}(\tilde{D}+\tilde{\varepsilon}_d)} - \frac{\tilde{\Gamma}_{0,+}}{\mathcal{E}(\tilde{D}-\tilde{\varepsilon}_d)} + \frac{\tilde{\Gamma}_{2,+}}{\mathcal{E}(\tilde{D}-\tilde{U}-\tilde{\varepsilon}_d)} - \frac{\tilde{\Gamma}_{2,-}}{\mathcal{E}(\tilde{D}+\tilde{U}+\tilde{\varepsilon}_d)}\right] + O(V^3). \quad \text{(A19)}$$

The band-edge hybridization functions $\tilde{\Gamma}_\tau$ rescale both due to the replacement of D by $\tilde{D}$ in Eq. (4) and due to the perturbative corrections to $V_{\tau,\mathbf{k}}$ in Eq. (A17), leading to the scaling equation

$$\frac{d\tilde{\Gamma}_{\tau,\pm}}{d\tilde{D}} = r\,\frac{\tilde{\Gamma}_{\tau,\pm}}{\tilde{D}} + O(V^4). \quad \text{(A20)}$$

The bare hybridization functions specified in Eq. (A4) are such that $\tilde{\Gamma}_{\tau,\pm}(D) = \Gamma$. For $r > 0$, moreover, Eq. (A20) shows that the band-edge hybridization functions are irrelevant (in the RG sense), and so too must be any differences among the renormalized values of the four hybridization widths. It is therefore an excellent approximation to set $\tilde{\Gamma}_{\tau,\pm} = \tilde{\Gamma}$ from the outset, leading to the simplified scaling equations given in Eqs. (16)–(18).

*mxcheng@phys.ufl.edu

[1] S. L. Sondhi, S. M. Girvin, J. P. Carini, and D. Shahar, Rev. Mod. Phys. **69**, 315 (1997).
[2] S. Sachdev, *Quantum Phase Transitions* (Cambridge University Press, Cambridge, UK, 1999).
[3] P. W. Anderson, Science **235**, 1196 (1987).
[4] E. Dagotto, Rev. Mod. Phys. **66**, 763 (1994).
[5] D. M. Broun, Nat. Phys. **4**, 170 (2008).
[6] P. Gegenwart, Q. Si, and F. Steglich, Nat. Phys. **4**, 186 (2008).
[7] Q. Si and F. Steglich, Science **329**, 1161 (2010).
[8] T. Giamarchi, C. Rüegg, and O. Tchernyshov, Nat. Phys. **4**, 196 (2008).
[9] V. Dobrosavljević, in *Conductor-Insulator Quantum Phase Transitions*, edited by V. Dobrosavljević, N. Trivedi, and J. M. Valles, Jr. (Cambridge University Press, Cambridge, UK, 2012), Chap. 1; also available as arXiv:1112.6166.
[10] M. Vojta, Philos. Mag. **86**, 1807 (2006).
[11] D. Withoff and E. Fradkin, Phys. Rev. Lett. **64**, 1835 (1990).
[12] C. Gonzalez-Buxton and K. Ingersent, Phys. Rev. B **54**, R15614 (1996).
[13] R. Bulla, Th. Pruschke, and A. C. Hewson, J. Phys.: Condens. Matter **9**, 10463 (1997).
[14] C. Gonzalez-Buxton and K. Ingersent, Phys. Rev. B **57**, 14254 (1998).
[15] D. E. Logan and M. T. Glossop, J. Phys.: Condens. Matter **12**, 985 (2000).
[16] R. Bulla, M. T. Glossop, D. E. Logan, and Th. Pruschke, J. Phys.: Condens. Matter **12**, 4899 (2000).
[17] M. T. Glossop and D. E. Logan, J. Phys.: Condens. Matter **15**, 7519 (2003).
[18] M. Sigrist and K. Ueda, Rev. Mod. Phys. **63**, 239 (1991).
[19] B. A. Volkov and O. A. Pankratov, Pis'ma Zh. Eksp. Teor. Fiz. **42**, 145 (1985) [JETP Lett. **42**, 178 (1985)].
[20] L. G. G. V. Dias da Silva, N. P. Sandler, K. Ingersent, and S. E. Ulloa, Phys. Rev. Lett. **97**, 096603 (2006).
[21] L. G. G. V. Dias da Silva, K. Ingersent, N. Sandler, and S. E. Ulloa, Phys. Rev. B **78**, 153304 (2008).
[22] L. G. G. V. Dias da Silva, N. Sandler, P. Simon, K. Ingersent, and S. E. Ulloa, Phys. Rev. Lett. **102**, 166806 (2009).
[23] K. Ingersent and Q. Si, Phys. Rev. Lett. **89**, 076403 (2002).
[24] M. Kircán and M. Vojta, Phys. Rev. B **69**, 174421 (2004).
[25] L. Fritz and M. Vojta, Phys. Rev. B **70**, 214427 (2004).
[26] W. Hofstetter and H. Schoeller, Phys. Rev. Lett. **88**, 016803 (2001).
[27] Y. Oreg and D. Goldhaber-Gordon, Phys. Rev. Lett. **90**, 136602 (2003).
[28] M. Pustilnik, L. Borda, L. I. Glazman, and J. von Delft, Phys. Rev. B **69**, 115316 (2004).
[29] M. R. Galpin, D. E. Logan, and H. R. Krishnamurthy, Phys. Rev. Lett. **94**, 186406 (2005).
[30] R. Žitko and J. Bonča, Phys. Rev. B **74**, 045312 (2006).
[31] D. E. Logan, C. J. Wright, and M. R. Galpin, Phys. Rev. B **80**, 125117 (2009).
[32] A. Wong, W. B. Lane, L. G. G. V. Dias da Silva, K. Ingersent, N. Sandler, and S. E. Ulloa, Phys. Rev. B **85**, 115316 (2012).
[33] R. M. Potok, I. G. Rau, H. Shtrikman, Y. Oreg, and D. Goldhaber-Gordon, Nature (London) **446**, 167 (2007).
[34] N. Roch, S. Florens, V. Bouchiat, W. Wernsdorfer, and F. Balestro, Nature (London) **453**, 663 (2008).
[35] H. Park, J. Park, A. K. L. Lim, E. H. Anderson, A. P. Alivisatos, and P. L. McEuen, Nature (London) **407**, 57 (2000).
[36] E. M. Weig, R. H. Blick, T. Brandes, J. Kirschbaum, W. Wegscheider, M. Bichler, and J. P. Kotthaus, Phys. Rev. Lett. **92**, 046804 (2004).
[37] P. W. Anderson, Phys. Rev. **124**, 41 (1961).
[38] T. Holstein, Ann. Phys. (NY) **8**, 325 (1959).
[39] H. Kaga, I. Sato, and M. Kobayashi, Prog. Theor. Phys. **64**, 1918 (1980).
[40] K. Schönhammer and O. Gunnarsson, Phys. Rev. B **30**, 3141 (1984).
[41] B. Alascio, C. Balseiro, G. Ortíz, M. Kiwi, and M. Lagos, Phys. Rev. B **38**, 4698 (1988)
[42] T. Östreich, Phys. Rev. B **43**, 6068 (1991).
[43] A. C. Hewson and D. Meyer, J. Phys.: Condens. Matter **14**, 427 (2002).
[44] G. S. Jeon, T.-H. Park, and H.-Y. Choi, Phys. Rev. B **68**, 045106 (2003).
[45] J.-X. Zhu and A. V. Balatsky, Phys. Rev. B **67**, 165326 (2003).
[46] H. C. Lee and H.-Y. Choi, Phys. Rev. B **69**, 075109 (2004); **70**, 085114 (2004).
[47] E. Šimánek, Solid State Commun. **32**, 731 (1979).
[48] C. S. Ting, D. N. Talwar, and K. L. Ngai, Phys. Rev. Lett. **45**, 1213 (1980).
[49] H.-B. Schüttler and A. J. Fedro, Phys. Rev. B **38**, 9063 (1988).
[50] P. S. Cornaglia, H. Ness, and D. R. Grempel, Phys. Rev. Lett. **93**, 147201 (2004).
[51] P. S. Cornaglia, D. R. Grempel, and H. Ness, Phys. Rev. B **71**, 075320 (2005).

[52]S. Andergassen, T. A. Costi, and V. Zlatić, Phys. Rev. B **84**, 241107(R) (2011).

[53]Equation (2a) is equivalent, apart from an additive constant $-\varepsilon_d$, to the more conventional form Eq. (A2). The form of Eq. (2a) emphasizes the charge-conjugation symmetry of the full Hamiltonian [Eq. (1)] in the special case $\delta_d = 0$.

[54]The hybridization *function* is denoted by a bold symbol $\mathbf{\Gamma}$ to distinguish it from the hybridization *width* Γ appearing on the right-hand side of Eq. (4).

[55]H. R. Krishna-murthy, J. W. Wilkins, and K. G. Wilson, Phys. Rev. B **21**, 1003 (1980); **21**, 1044 (1980).

[56]The impurity contribution to a physical property is defined in the standard manner (see, e.g., Ref. 55) as the difference between the total value of the property for the system including the impurity and the total value of the same property for the host alone. In the case of the Anderson-Holstein model (with or without a pseudogap), we treat the local-boson mode as part of the host. As a result, the impurity entropy takes a finite value $S_{\rm imp} = \ln 4$ in the high-temperature limit.

[57]Extension of the analysis in Sec. IV of Ref. 14 indicates that in the vicinity of the symmetric strong-coupling fixed point of the pseudogap Anderson model, breaking time-reversal symmetry admits a relevant perturbing operator $O_{H_1} = \frac{1}{2}\Lambda^{N/2}(f^\dagger_{1\uparrow} f_{1\uparrow} - f^\dagger_{1\downarrow} f_{1\downarrow}) \propto T^{-\min(r,1)}$ where the $f_{n\sigma}$ is one of the annihilation operators entering Eq. (22). By contrast, the leading perturbation introduced near the asymmetric strong-coupling fixed point is an irrelevant operator $O_{H_2} = \frac{1}{2}\Lambda^{N/2}(f^\dagger_{2\uparrow} f_{2\uparrow} - f^\dagger_{2\downarrow} f_{2\downarrow}) \propto T^r$.

[58]This conclusion contradicts Ref. 25 but is supported by numerical renormalization-group calculations (Ref. 62).

[59]J. R. Schrieffer and P. A. Wolff, Phys. Rev. **149**, 491 (1966).

[60]I. G. Lang and Y. A. Firsov, Zh. Eksp. Teor. Fiz. **43**, 1843 (1962) [Sov. Phys. JETP **16**, 1301 (1963)].

[61]F. D. M. Haldane, Phys. Rev. Lett. **40**, 416 (1978).

[62]M. Cheng and K. Ingersent (unpublished).

[63]I. S. Gradshteyn and I. M. Ryzhik, *Tables of Integrals, Series, and Products*, edited by A. Jeffrey and A. Zwillinger, 7th ed. (Academic, San Diego, 2007), Sec. 8.35.

[64]K. G. Wilson, Rev. Mod. Phys. **47**, 773 (1975).

[65]R. Bulla, T. A. Costi, and Th. Pruschke, Rev. Mod. Phys. **80**, 395 (2008).

[66]For any situation that does not obey $\tilde{\Gamma}(-\varepsilon) \neq \tilde{\Gamma}(\varepsilon)$ for all ε, the right-hand side of Eq. (22) must be augmented by a term $\sum_{n,\sigma} \Lambda^{-n/2} e_n f^\dagger_{n\sigma} f_{n\sigma}$, where the onsite energies e_n parametrize the particle-hole asymmetry of the hybridization function.

[67]K. Ingersent, Phys. Rev. B **54**, 11936 (1996).

[68]S. Sachdev, Z. Phys. B: Condens. Matter **94**, 469 (1994).

[69]M. Vojta and R. Bulla, Phys. Rev. B **65**, 014511 (2001).